TCAB1 prevents nucleolar accumulation of the telomerase RNA to promote telomerase assembly

Basma S. Al-Masraf [1,2,3], Gloria I. Perez [1], Kate Adams-Boone [1], Scott B. Cohen [4], Li Han [5], Kefei Yu [5], Jens C. Schmidt [1,6,*]

[1] Institute for Quantitative Health Sciences and Engineering, Michigan State University, East Lansing, MI, U.S.A.

[2] College of Osteopathic Medicine, Michigan State University, East Lansing, MI, U.S.A.

[3] Cellular and Molecular Biology Graduate Program, College of Natural Sciences, Michigan State University, East Lansing, MI, U.S.A.

[4] Children's Medical Research Institute and University of Sydney, Westmead, NSW 2145, Australia.

[5] Department of Microbiology and Molecular Genetics, Michigan State University, East Lansing, MI, U.S.A.

[6] Department of Obstetrics, Gynecology, and Reproductive Biology.

[*] Correspondence: schmi706@msu.edu

Abstract

Localization of a wide variety of RNAs to non-membrane bound cellular compartments such as nucleoli, Cajal bodies, and stress-granules is critical for their function and stability. The molecular mechanisms that underly the recruitment and exclusion of specific RNAs from these phase-separated organelles is poorly understood. Telomerase is a ribonucleoprotein (RNP), that is composed of the reverse transcriptase protein TERT, the telomerase RNA (TR), and several auxiliary proteins that associate with TR, including TCAB1. Here we show that, that in the absence of TCAB1, TR is trapped in the nucleolus, while TERT localizes to the nucleoplasm and is excluded from the nucleolus, which prevents telomerase assembly. Thus, nucleolar phase separation constitutes a barrier that counteracts telomerase assembly and TCAB1 is required to exclude the telomerase RNA from the nucleolus. Our work provides general insight into the mechanism and functional consequences of RNA recruitment to non-membrane bound organelles and proposes a new model explaining the critical role of TCAB1 in telomerase function.

Introduction

Human cells contain a number of non-membrane bound organelles that carry out critical cellular functions. For instance, nucleoli and Cajal bodies are phase-separated nuclear organelles that play important roles in the biogenesis and maturation of many cellular RNAs (Hyman et al., 2014; Mitrea and Kriwacki, 2016). Nucleoli and Cajal bodies contain a wide range of small nucleolar and small Cajal body-specific RNAs (snoRNAs and scaRNAs, respectively). A subset of these snoRNAs and scaRNAs are bound by the H/ACA complex, which contains NOP10, NHP2, GAR1, and the pseudouridylase dyskerin, which modifies ribosomal and spliceosomal RNA precursors and other RNAs (Angrisani et al., 2014). A key difference between snoRNAs and scaRNAs is the presence of the Cajal-body box (CAB-box) motif in scaRNAs that directly associates with the telomerase Cajal body protein 1 (TCAB1, also known as WRAP53) (Jády et al., 2004; Schmidt and Cech, 2015; Venteicher et al., 2009). TCAB1 is required for the recruitment of scaRNAs to Cajal bodies and in its the absence scaRNAs localize to the nucleolus (Venteicher et al., 2009). Therefore, TCAB1 controls which phase-separated nuclear organelle scaRNAs associate with. Importantly, the molecular mechanism by which TCAB1 drives exclusion of scaRNAs from the nucleolus and facilitates their recruitment to Cajal bodies is unknown. In addition, it is unclear whether miss-localization of scaRNAs to the nucleolus has functional consequences.

The telomerase RNA (TR) is a scaRNA and like other scaRNAs its association with nucleoli and Cajal bodies is controlled by TCAB1 (Schmidt and Cech, 2015). Telomere maintenance by telomerase is essential for continuous proliferation of stem cell

57 populations in the human body and most cancers require telomerase activity for their
58 survival (Stewart and Weinberg, 2006). To compensate for the incomplete replication of
59 chromosome ends, telomerase appends TTAGGG repeats to the telomeric single-
60 stranded overhang (Schmidt and Cech, 2015). Telomerase-mediated telomere
61 maintenance requires three critical steps: Telomerase assembly, telomerase recruitment
62 to telomeres, and telomeric repeat synthesis (Schmidt and Cech, 2015). Mutations in
63 several genes have been identified that cause deficiencies in one of these critical steps
64 and lead to a variety of diseases known as telomere syndromes, characterized by
65 premature depletion of stem cell populations (Armanios and Blackburn, 2012). In addition,
66 telomerase is inappropriately activated in >85% of cancers (Stewart and Weinberg,
67 2006). While telomerase recruitment to telomeres (Nandakumar and Cech, 2013) and
68 telomerase catalysis (Wu et al., 2017) have been studied extensively, much less is known
69 about telomerase assembly. Importantly, telomerase assembly could be targeted to
70 reduce telomerase activity in cancer cells, or to increase telomerase function in patients
71 affected by genetically defined telomerase deficiency syndromes (Nagpal et al., 2020;
72 Shukla et al., 2020).
73
74 Telomerase is a complex ribonucleoprotein (RNP). The core components of telomerase
75 are the telomerase reverse transcriptase (TERT) protein, TR, the H/ACA complex, and
76 TCAB1 (Schmidt and Cech, 2015). The primary function of the H/ACA complex is to
77 stabilize TR, by directly binding to its 3'-end, preventing the exonucleolytic degradation of
78 TR (Stuart et al., 2015; Tummala et al., 2015). The 3'-end formation of TR is tightly
79 regulated by the competing activities of the poly-(A) polymerase PAPD5 and the nuclease

80 PARN (Shukla et al., 2016; Tseng et al., 2015). Loss of TCAB1 function leads to telomere
81 attrition in a variety of cell lines (Chen et al., 2018; Venteicher et al., 2009; Vogan et al.,
82 2016; Zhong et al., 2011). In addition, multiple mutations in TCAB1 have been identified
83 that cause misfolding of TCAB1 and lead to dyskeratosis congenita, a telomere syndrome
84 (Freund et al., 2014; Zhong et al., 2011). While these observations highlight that TCAB1
85 is necessary for telomere maintenance, the underlying molecular mechanism is unclear.
86 Initially, it was proposed that TCAB1 is required for telomerase recruitment to telomeres
87 (Stern et al., 2012; Venteicher et al., 2009). A more recent study suggested that TCAB1
88 is required for the correct folding of TR, and that its absence causes a reduction in
89 telomerase activity (Chen et al., 2018). Importantly, all previous studies have come to the
90 conclusion that TCAB1 is not required for telomerase assembly.
91
92 Here we analyze telomerase assembly in intact cells and by purification of the telomerase
93 RNP and demonstrate that, contrary to previous findings, TCAB1 promotes telomerase
94 assembly *in vivo.* Using a combination of genetic perturbations, biochemical analysis of
95 telomerase function, cell biological approaches, and single-molecule live cell imaging, we
96 show that in the absence of TCAB1, TR is sequestered in the nucleolus while TERT is
97 excluded from the nucleolus. The spatial separation of TERT and TR that we observe in
98 our experiments is inconsistent with proper telomerase assembly. Furthermore, we show
99 that the limited amount of telomerase that can assemble in the absence of TCAB1 is fully
100 active and can localize to telomeres, suggesting that TCAB1 is not required for the
101 enzymatic function of telomerase or its recruitment to telomeres. In addition, we
102 demonstrate that the diffusion properties of TERT in cells that lack TCAB1 closely

103 resemble those of TERT that is not bound to TR. We conclude that the sequestration of
104 TR in the nucleolus, when TCAB1 is absent, prevents its association with TERT, and that
105 this lack of telomerase assembly is the molecular mechanism underlying the critical role
106 of TCAB1 in telomere maintenance. Our results also demonstrate that the nucleolar
107 phase separation constitutes a barrier for telomerase assembly and suggest that
108 incompletely assembled RNPs are tightly associated with the nucleolus and do not readily
109 enter the nucleoplasm.
110

Results

Loss of TCAB1 leads to nucleolar accumulation of TR

To confirm that TR is sequestered in the nucleolus in the absence of TCAB1, we attempted to knock-out TCAB1 in parental HeLa cells and HeLa cells expressing 3xFLAG-HaloTag-TERT and mEos3.2-TRF2 from the endogenous *TERT* and *TRF2* loci (referred to as Halo-TERT from here on) using Cas9 and a single guide RNA targeting the first exon of the *TCAB1* locus (Figure 1 – figure supplement 1). We isolated clonal cell lines that lacked a wild-type *TCAB1* allele (Figure 1 – figure supplement 1) and analyzed TCAB1 expression using Western blot. While a TCAB1 antibody targeting the N-terminus of TCAB1 failed to detect TCAB1 in our knock-out clones (Figure 1 – figure supplement 1), antibodies raised against more C-terminal TCAB1 fragments detected a truncated form of TCAB1 (Figure 1 – figure supplement 1). The size of the truncated TCAB1 is consistent with the use of methionine 129 as an alternative start codon. Importantly, the truncated form of TCAB1 localizes to Cajal bodies (Figure 1 – figure supplement 1) and scaRNA localization is unaffected in its presence (Figure 1 – figure supplement 1), indicating that it is at least partially functional. To avoid expression of the truncated TCAB1 variant, we knocked out TCAB1 using Cas9 with two guide RNAs to delete exons 2 and 3 from the TCAB1 gene, which removes the coding sequence for residues 144-214 of TCAB1 and results in a frame shift (Figure 1 – figure supplement 2). TCAB1 knock-out was validated by Southern blot, PCR, Western blot, and immunofluorescence imaging (IF, Fig. 1A-C, Figure 1 – figure supplement 2). Fluorescence *in situ* hybridization (FISH) demonstrated that TR accumulates in the nucleolus in cells that lack TCAB1, as indicated by co-localization of TR and nucleolar dyskerin signals. Importantly, expression of GFP-

134 TCAB1 in TCAB1 knock-out cells rescued TR localization to Cajal bodies (Figure 1 –
135 figure supplement 2), confirming that the miss-localization of TR to nucleoli is caused by
136 absence of TCAB1. These observations confirm that TCAB1 is required to prevent TR
137 accumulation in the nucleolus (Fig. 1C).

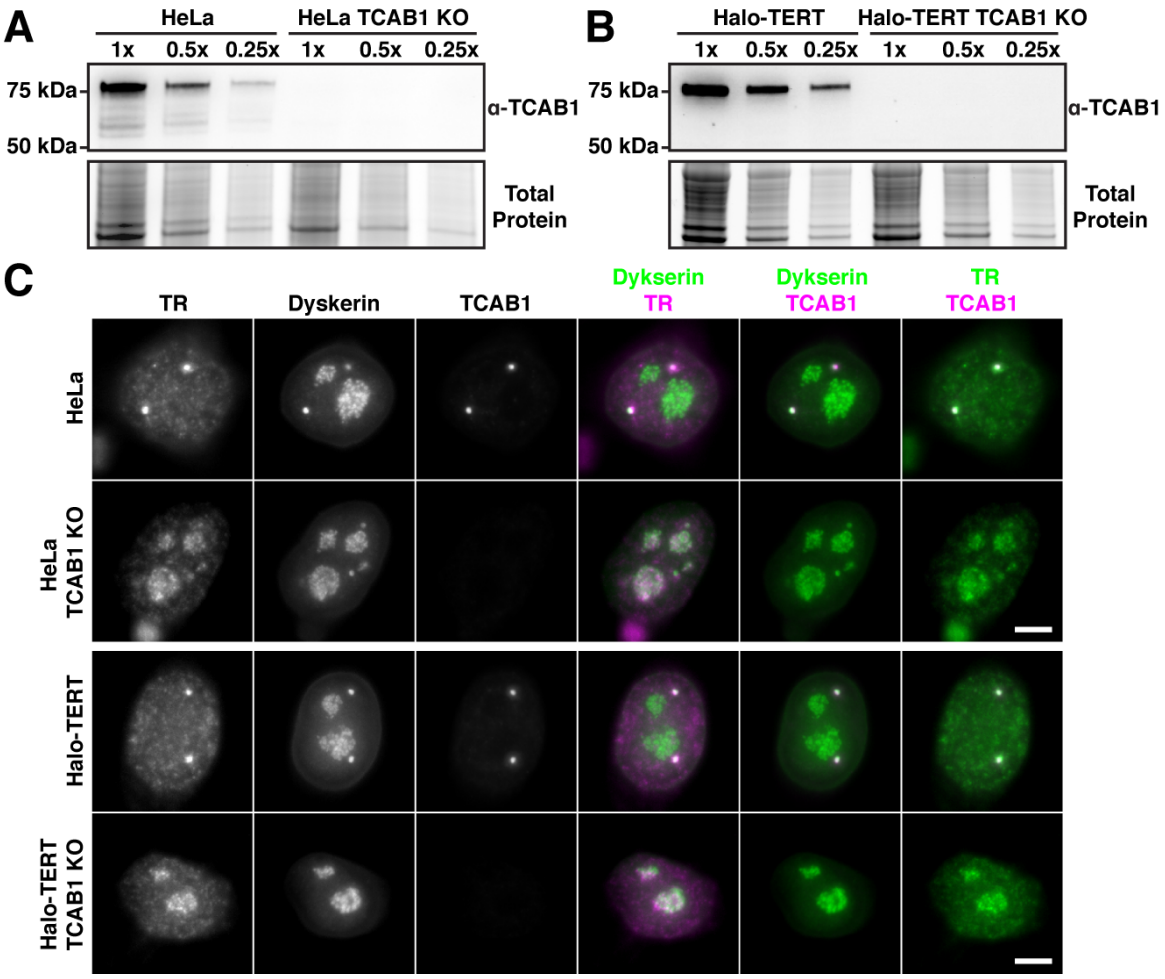

138

Figure 1. TR is localized to nucleoli in TCAB1 knock-out cells. (A-B) Western blot demonstrating the absence of TCAB1 protein in TCAB1 knock-out cell lines generated from **(A)** HeLa and **(B)** Halo-TERT parental cell lines (probed with Proteintech TCAB1 antibody). **(C)** Immuno-fluorescence with anti-dyskerin and anti-TCAB1 antibodies coupled to fluorescence in-situ hybridization with probes against TR, demonstrating the absence of TCAB1 and TR localization to nucleoli in TCAB1 knock-out cells (scale bar = 5 μm).

139 **TERT is excluded from nucleoli**

140 Our previous observations demonstrated that TERT does not enter nucleoli in human
141 cancer cells (Schmidt et al., 2016). To confirm these results, we performed single-

142 molecule imaging of 3xFLAG-HaloTag-TERT in living HeLa cells. Consistent with our
143 previous results, 3xFLAG-HaloTag-TERT was not observed entering or overlapping with
144 nucleoli, which are discernible as circular shapes in the nucleus under transmitted light

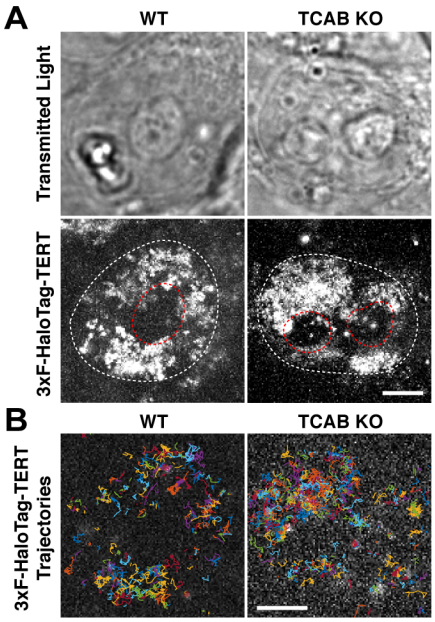

Figure 2. TERT is excluded from nucleoli in control and TCAB1 knock-out cells. (A) Maximum intensity projections of 2000 frames of 3xFLAG-HaloTag (JF646) TERT movies (bottom), demonstrating that the TERT signal does not overlap with the nucleolus detected as circular shape in the transmitted light image in control and TCAB1 knock-out cells (top, red dashed line, scale bar = 2 μm). **(B)** TERT particle trajectories from the cells shown in Fig. 2A, demonstrating that TERT molecules move parallel to or away from the nucleolus when located at the interface between the nucleolus and nucleoplasm.

145
146 illumination (Fig. 2A,B, Figure 2 – figure supplement 1, Movie 1,2). TERT trajectories in
147 close proximity to nucleoli revealed that their movement is biased away from the
148 nucleolus, suggesting that TERT is repelled by the nucleolus (Fig. 2B). To exclude the
149 possibility that nucleolar exclusion is a consequence of the 3xFLAG-HaloTag on the N-
150 terminus of TERT used in our experiments, we transiently expressed the 3xFLAG-
151 HaloTag fused to a nuclear localization sequence (NLS) in HeLa cells. Single-molecule
152 imaging demonstrated that the nuclear 3xFLAG-HaloTag signals overlapped with the
153 nucleolus (Figure 2 – figure supplement 1, Movie 3). Similar to the 3xFLAG-HaloTag
154 alone, 3xFLAG-HaloTag-dyskerin also localized to the nucleolus (Figure 2 – figure
155 supplement 1). These results demonstrate that 3xFLAG-HaloTag-TERT is excluded from
156 the nucleolus and that this exclusion is not caused by the 3xFLAG-HaloTag but instead
157 is an intrinsic property of the TERT protein.

158

159 **TERT and TR localize to distinct nuclear compartments in cells lacking TCAB1**

160 It is well established that telomerase assembly is incomplete in human cancer cells, which
161 leads to substantial pools of TERT and TR that are not assembled into telomerase RNPs
162 (Xi and Cech, 2014). Together with our observation that TERT molecules rarely enter the
163 nucleolus (Schmidt et al., 2016) this suggests that both free TERT and assembled
164 telomerase RNPs do not enter the nucleolus. To test whether, like TR, TERT accumulates
165 in the nucleolus in cells lacking TCAB1, we carried out single-molecule imaging of
166 3xFLAG-HaloTag-TERT. Strikingly, TERT localization is unchanged in cells lacking
167 TCAB1 (Fig. 2A,B). This suggests that unlike TR, TERT does not accumulate in nucleoli
168 when TCAB1 is absent.

169 The experiments described so far demonstrate that TCAB1 is enriched in nucleoli
170 and TERT is excluded from nucleoli in cells lacking TCAB1, but they do not
171 simultaneously detect TERT and TR in the same cell. To overcome this limitation, we
172 over-expressed mCherry-TERT and TR in TCAB1 knock-out cells. In controls, TERT and
173 TR colocalized with dyskerin at telomeres marked by TRF2 (Fig. 3A). In addition, analysis
174 of the TERT signal across the nucleus and nucleolus revealed that TERT was depleted
175 from the nucleolus (Fig. 3B). Importantly, mCherry-dyskerin localized to the nucleolus,
176 demonstrating that the mCherry-tag does not lead to nucleolar exclusion of its fusion
177 partner (Figure 3 – figure supplement 1). In cells lacking TCAB1, mCherry-TERT was
178 diffusely localized in the nucleoplasm, localized to a subset of telomeres, and was
179 depleted from the nucleolus (Fig. 3A,C). Similar to endogenous TR, overexpressed TR

180 was enriched in the nucleolus in TCAB1 knock-out cells (Fig. 3A). In addition, TR was

181 frequently co-localized

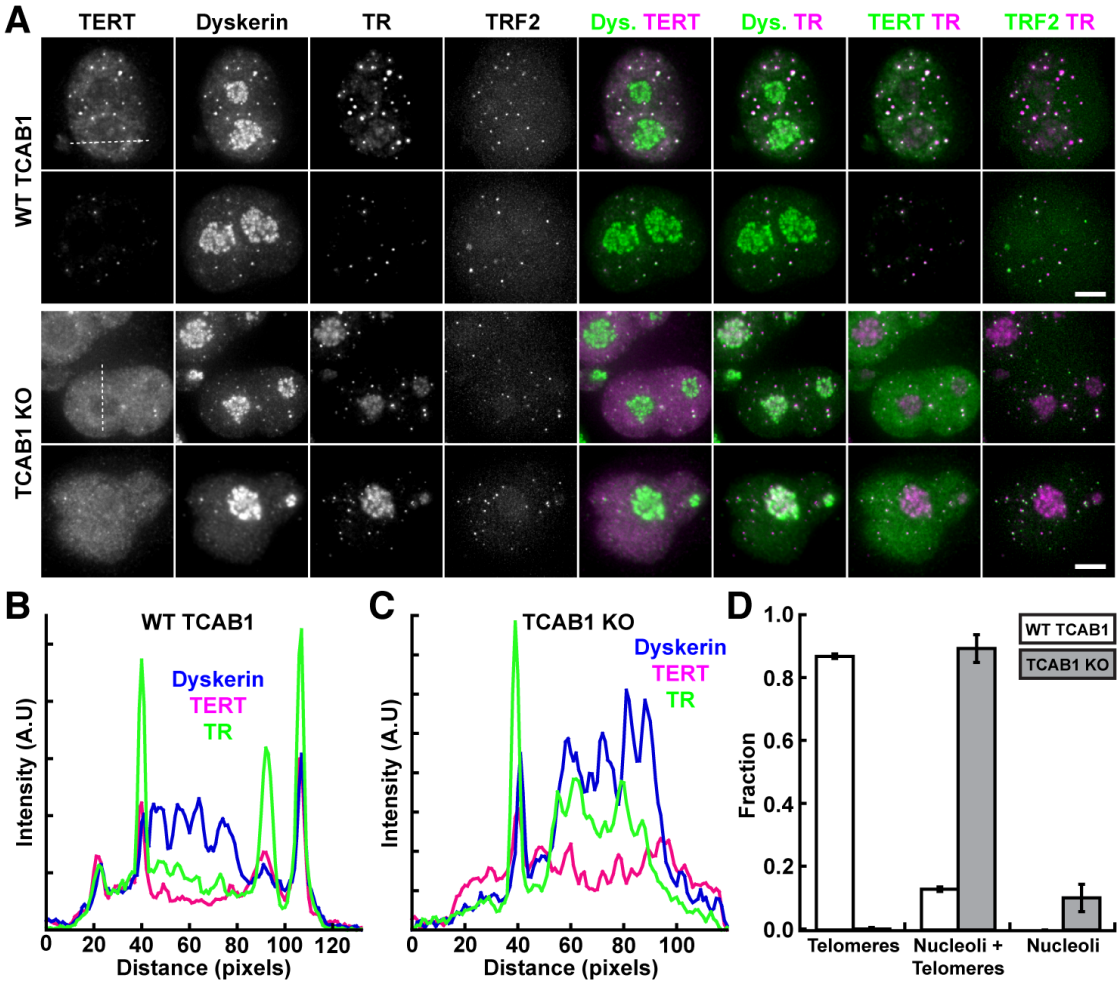

182

Figure 3. TERT and TR localize to distinct nuclear compartments in TCAB1 knock-out cells. (A) IF-FISH images of control and TCAB1 knock-out HeLa cells (3xFLAG-Halo-TERT, mEOS3.2-TRF2) overexpressing mCherry-TERT and TR (scale bar = 5 μm). Cells were probed with antibodies against dyskerin and mCherry, and FISH probes specific to TR. The intrinsic fluorescence of mEOS3.2-TRF2 was used to detect telomeres. TR and TERT are co-localized at telomeres in control cells. In TCAB1 knock-out cells, TR is enriched in nucleoli, while TERT is depleted from nucleoli in both control and TCAB1 knock-out cells. Both TERT and TR also localize to telomeres in TCAB1 knock-out cells. **(B-C)** Line scans of **(B)** control and **(C)** TCAB1 knock-out cells along the dashed white lines in Fig. 3A, demonstrating the enrichment of TR (green) in nucleoli (blue) in TCAB1 knock-out cells and the depletion of TERT (magenta) from nucleoli in both control and TCAB1 knock-out cells. **(D)** Quantification of the fraction of cells showing TR localization exclusively to telomeres, to telomeres and nucleoli, or only to nucleoli in cells over-expressing mCherry-TERT and TR (3 independent experiments, >100 cells per experiments, mean ± standard deviation).

183 with telomeres when mCherry-TERT and TR were overexpressed in cells that lack

184 TCAB1 (Fig. 3A,C-D). Similar TR localization patterns were found when overexpressing

185 untagged TERT and TR (Figure 3 – figure supplement 1) and untagged TERT was
186 excluded from nucleoli, confirming that nucleolar exclusion is an intrinsic property of
187 TERT (Figure 3 – figure supplement 1). Together these results demonstrate that, when
188 overexpressed in TCAB1 knock-out cells, TR is enriched in nucleoli and TERT is depleted
189 from nucleoli, consistent with a failure of nucleolar TR to assemble with TERT. In addition,
190 our observations suggest that overexpression can partially overcome the sequestration
191 of TR in the nucleolus when TCAB1 is absent, allowing a fraction of TR to bind to TERT
192 and localize to telomeres.
193
194 **TCAB1 promotes telomerase RNP assembly**
195 Previous studies by other laboratories have concluded that telomerase assembly is
196 unaffected by the absence of TCAB1 and whether TCAB1 is required for telomerase
197 activity is controversial (Chen et al., 2018; Venteicher et al., 2009; Vogan et al., 2016).
198 To assess the role of TCAB1 in telomerase assembly, we overexpressed TERT and TR
199 in parental HeLa and TCAB1 knock-out cells and immuno-purified TERT using a well-
200 established anti-TERT antibody (Cohen et al., 2007). To quantify telomerase assembly,
201 we measured TERT levels by Western blot and determined the amount of TR co-purified
202 using Northern blot (Fig. 4A,B). The amount of TR associated with TERT purified from
203 TCAB1 knock-out cells was significantly reduced compared to parental cells, for both
204 HeLa (31 $\pm$ 9%, mean $\pm$ SEM, $p = 0.001$) and Halo-TERT (33 $\pm$ 4%, mean $\pm$ SEM, $p =$
205 0.001) cell lines (Fig. 4D). As a second measure of telomerase RNP assembly we
206 quantified the amount of dyskerin associated with TERT (Fig. 4C). Since TR bridges
207 TERT and dyskerin, dyskerin co-purified with TERT directly reports on the presence of

208 TR. Consistent with the reduction in TR, the amount of dyskerin bound to TERT was also
209 significantly reduced when purified from cells lacking TCAB1 compared to parental
210 controls for both HeLa (22 ± 8%, mean ± SEM, p = 0.002) and Halo-TERT (32 ± 9%,
211 mean ± SEM, p = 0.004) cell lines (Fig. 4C,E). Importantly, we also confirmed that TCAB1

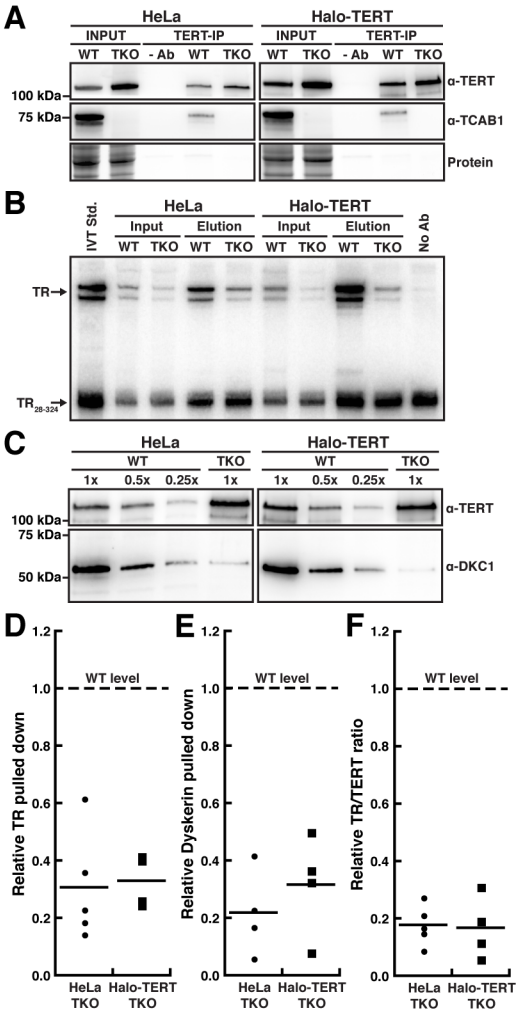

Figure 4. Telomerase Assembly is reduced in the absence of TCAB1. (A) Western blots analyzing TERT immuno-purification (using a sheep anti-TERT antibody) probed with a rabbit anti-TERT antibody (Abcam) and a TCAB1 antibody. **(B)** Northern blot of RNA extracted from input and purified TERT samples probed with three radiolabeled DNA oligonucleotides complementary to TR. Standards are *in vitro* transcribed full-length TR and truncated $TR_{28\text{-}324}$. $TR_{28\text{-}324}$ was added to samples prior to RNA extraction as loading and recovery control. **(C)** Western blots to analyze immuno-purified telomerase RNP composition. A single membrane was cut into two pieces that were probed with TERT and dyskerin antibodies, respectively. **(D-F)** Quantification of the amount of **(D)** TR, **(E)** dyskerin, and **(F)** the ratio of TR to TERT in TERT purifications from TCAB1 knock-out cells compared to parental controls (n = 4-5, mean). The dashed lines indicate the level in telomerase purified from wild-type TCAB1 control cells which was normalized to 1.0.

212
213 is absent from telomerase purified from TCAB1 knock-out cells (Fig. 4A). As a final
214 measure of telomerase assembly, we determined the ratio between TR and TERT (Fig.
215 4A,B,F), which was also significantly reduced when TERT was purified from TCAB1
216 knock-out cells (HeLa: 18 ± 3%, mean ± SEM, p < 0.001, Halo-TERT: 17 ± 5%, mean ±
217 SEM, p < 0.001). Altogether, these results demonstrate that telomerase assembly is

218 significantly reduced in the absence of TCAB1 and that overexpression of TERT and TR

219 is not sufficient to overcome this defect in telomerase RNP formation.

220

221 **TCAB1 is not required for telomerase catalytic activity**

222 Previous work by others has suggested that the defects in telomere maintenance

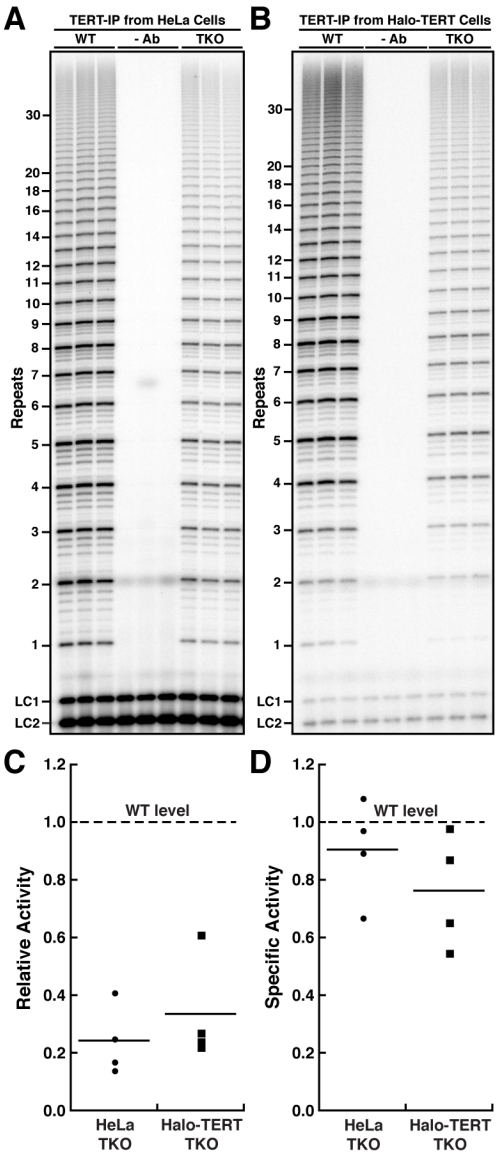

Figure 5. The specific activity of telomerase is unchanged in the absence of TCAB1. (A-B) Direct telomerase extension assay of telomerase immuno-purified from parental (WT) and TCAB1 knock-out (TKO) **(A)** HeLa and **(B)** Halo-TERT cell lines. LC1 and LC2, radiolabeled DNA oligonucleotide loading controls. In - Ab samples the TERT antibody was omitted during the immuno-purification. **(C)** Quantification of telomerase activity in samples from TCAB1 knock-out cells relative to parental controls (n = 4, mean). **(D)** Specific activity of telomerase purified from TCAB1 knock-out cells relative to parental controls (n = 4, mean). Specific activity was calculated by dividing the relative activity (see Fig. 5C) by the relative amount of TR present in immuno-purified TERT samples (see Fig. 4D). The dashed lines indicate the activity level in telomerase purified from wild-type TCAB1 control cells which was normalized to 1.0.

223

224 observed in TCAB1 knock-out cells are the consequence of reduced telomerase activity
225 caused by the miss-folding of the telomerase RNA rather than impaired telomerase
226 assembly (Chen et al., 2018). This TR folding model predicts that the specific activity of
227 telomerase is reduced. To determine the specific activity of telomerase purified from
228 TCAB1 knock-out cells, we measured telomerase activity using the direct telomerase
229 extension assays (Fig. 5A,B, Figure 5 – figure supplement 1), and divided the activity by
230 the amount of TR in the respective telomerase sample (Fig. 4B,D), which is a direct
231 measure of the quantity of telomerase RNP present. Total activity of telomerase purified
232 from TCAB1 knock-out cells was significantly reduced relative to telomerase purified from
233 parental controls telomerase (Fig. 5C, HeLa: 24 ± 6%, mean ± SEM, $p < 0.001$, Halo-
234 TERT: 34 ± 9%, mean ± SEM, $p = 0.005$), consistent with observations by others (Chen
235 et al., 2018). In contrast, the specific activity of telomerase derived from cells that lack
236 TCAB1 was not significantly reduced compared to controls (Fig. 5D, HeLa: 90 ± 9%, mean
237 ± SEM, $p = 0.35$, Halo-TERT: 76 ± 10%, mean ± SEM, $p = 0.1$). Together these
238 observations suggest that TCAB1 is required for telomerase assembly and that the limited
239 amount of telomerase RNP that can form in the absence of TCAB1 is fully active.
240

241 **TCAB1 is required for telomerase assembly in living cells**

242 The experiments presented thus far demonstrate that telomerase assembly is
243 significantly reduced in the absence of TCAB1 but were carried out in fixed cells or cell
244 lysates. To analyze telomerase assembly in intact cells, we carried out live cell single-
245 molecule imaging of 3xFLAG-HaloTag-TERT and determined the diffusion coefficient of
246 TERT particles (Fig. 6A, Movie 4, Figure 6 – figure supplement 1). The diffusion co-

247 efficient is a measure of the rate of movement of a molecule and depends on the size of
248 the complex it is part of and reports on molecular interactions formed with other sub-
249 cellular structures. Analysis of the diffusion coefficients of TERT trajectories in control
250 cells revealed three distinct populations of TERT particles (Fig. 6B-D). A static population
251 (D_S = 0.03 μm^2/s, 12%) which likely represents assembled telomerase RNPs bound to
252 telomeres or Cajal bodies, a slowly diffusion population (D_{F1} = 0.35 μm^2/s, 28%) and a
253 rapidly diffusing population (D_{F2} = 1.54 μm^2/s, 60%). The slowly diffusing population likely
254 includes assembled telomerase RNPs, while the rapidly diffusing particles represents
255 TERT molecules, which are not assembled with TR (Fig. 6B). Importantly, these diffusion
256 coefficients are largely consistent with our previous results using a distinct method to
257 determine their values (Schmidt et al., 2016). In the absence of TCAB1, the diffusion
258 coefficient of the freely diffusing TERT population was increased (D_{F2} = 1.78 ± 0.04 μm^2/s,
259 mean ± SEM, p = 0.04, Fig. 6C) and the fraction of the TERT populations that includes
260 assembled telomerase RNPs was significantly reduced ($F_{Slow+Static}$ = 29 ± 1%, mean ±
261 SEM, p = 0.02, Fig. 6D). This observation is consistent with our model that in the absence
262 of TCAB1, telomerase assembly is defective. To determine the degree to which
263 telomerase assembly is affected in cells lacking TCAB1, we knocked out TR, completely
264 abolishing telomerase assembly. TR knock-out was confirmed by PCR and Sanger
265 sequencing, FISH, and qPCR (Figure 6 – figure supplement 1). Similar to control cells
266 and TCAB1 knock-out cells, TERT was also excluded from nucleoli in cells lacking TR
267 (Fig. S6D). Strikingly, the diffusion coefficients and the fraction of slow and static TERT
268 particles in cells lacking TR closely resembled those of TCAB1 knockout cells (Fig. 6A-
269 D, Figure 6 – figure supplement 1, Movie 4-5). To analyze the

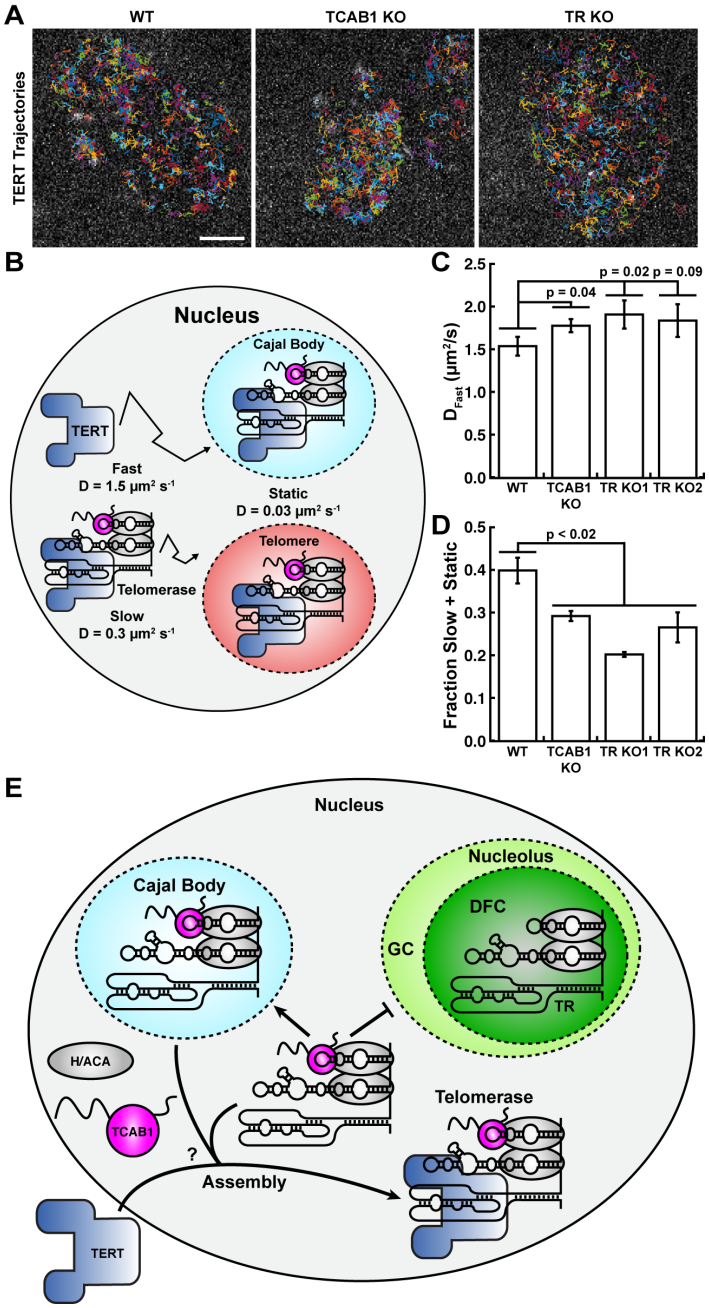

Figure 6. Telomerase assembly is reduced in TCAB1 knock-out cells. (A) TERT particle trajectories from control, TCAB1 knock-out, and TR knock-out cells expressing 3xFLAG-HaloTag TERT (JF646, scale bar = 2 μm). **(B)** Diagram of distinct populations of TERT particles detected in control cells. **(C)** Diffusion coefficient of the rapidly diffusing TERT population in control, TCAB1 knock-out, and TR knock-out cells (3 independent experiments, >15 cells per experiment per cell line, mean ± standard deviation, complete data in Fig. S6D). **(D)** Fraction of slow plus static TERT particles in control, TCAB1 knock-out, and TR knock-out cells expressing 3xFLAG-HaloTag TERT (3 independent experiments, >15 cells per experiment per cell line, mean ± standard deviation, complete data in Fig. S6D). **(D)** Model for the regulation of telomerase assembly by TCAB1. In the absence of TCAB1, TR is sequestered in the dense fibrillar component (DFC) of the nucleolus, which is separated from the nucleoplasm by the granular component (GC) of the nucleolus.

271 interaction of TERT with telomeres, we filtered out TERT trajectories that came into
272 proximity with telomeres marked by mEOS3.2-TRF2, as previously described (Schmidt
273 et al., 2016). To assess the interaction of TERT with telomeres, we plotted the step-size
274 vs. the distance from the closest telomere for each step of these trajectories (Figure 6 –
275 figure supplement 2). In control cells, we observed an enrichment of smaller step sizes
276 and particles in close proximity to telomeres, consistent with TERT interactions with the
277 telomere (Figure 6 – figure supplement 2). In contrast, TERT trajectories from TCAB1
278 knock-out cells lacked this enrichment, and the step size vs. distance from the closest
279 telomere plots were identical to those from TR knock-out cells (Figure 6 – figure
280 supplement 2). In addition, diffusion analysis using SpotOn revealed that the fraction of
281 static TERT particles at telomeres was reduced from 12% in control cells to 4-5% in
282 TCAB1 and TR knock-out cells (Figure 6 – figure supplement 2). These observations
283 indicate that in the absence of either TCAB1 or TR, stable interactions of telomerase with
284 telomeres occur at a lower frequency because they require base pairing of TR with the
285 chromosome end (Schmidt et al., 2018). Together these results demonstrate that
286 telomerase assembly is strongly reduced in the absence of TCAB1.
287
288

289 **Discussion**

290 The experiments described in this study demonstrate that TCAB1 promotes telomerase
291 assembly. In the absence of TCAB1 the telomerase RNA is targeted to the nucleolus via
292 its association with dyskerin and other components of the H/ACA complex. In contrast to
293 TR, TERT cannot enter the nucleolus, preventing its association with TR in cells that lack
294 TCAB1. This demonstrates that nucleolar phase separation counteracts telomerase
295 assembly. In addition, we demonstrate that sequestration of TR in the phase-separated
296 nucleolus in the absence of TCAB1 can be partially overcome by telomerase
297 overexpression, leading to telomerase assembly and localization to telomeres. This
298 suggests that the nucleolus has a limited capacity to accommodate cellular RNAs and
299 that TCAB1 is not required for telomerase recruitment to telomeres. Finally, we
300 demonstrate that while telomerase assembly is limited the specific activity of telomerase
301 is unchanged in the absence of TCAB1, which excludes a role of TCAB1 in telomerase
302 catalytic function. Altogether our work completely reshapes our understanding of the role
303 of TCAB1 in telomerase function in human cells and provides insight into the role phase-
304 separated organelles play in RNP assembly and function.

305

306 **TCAB1 promotes telomerase assembly**

307 The importance of TCAB1 for telomere maintenance is undisputed (Chen et al., 2018;
308 Venteicher et al., 2009). Knock-out or depletion of TCAB1 results in telomere shortening
309 (Chen et al., 2018; Venteicher et al., 2009; Vogan et al., 2016). All previous work also
310 concluded that TR is enriched in the nucleolus in the absence of TCAB1 (Chen et al.,
311 2018; Stern et al., 2012; Venteicher et al., 2009; Vogan et al., 2016; Zhong et al., 2011).

312 Finally, all prior studies propose that TCAB1 is not required for telomerase assembly but
313 instead plays a role telomerase trafficking to Cajal bodies and telomeres or is required for
314 telomerase catalysis (Chen et al., 2018; Stern et al., 2012; Venteicher et al., 2009; Vogan
315 et al., 2016; Zhong et al., 2011). In contrast, our results demonstrate that in the absence
316 of TCAB1, TERT and TR are localized to the distinct sub-cellular compartments, the
317 nucleoplasm and the nucleolus, respectively. This spatial separation strongly reduces
318 telomerase assembly, which leads to reduced number of telomerase RNPs per cell and
319 in turn telomere shortening. Our conclusions are based on a variety of quantitative
320 approaches analyzing telomerase assembly by purification of the telomerase RNP and in
321 intact cells. Analysis of TERT localization in living and fixed cells clearly demonstrates
322 that TERT is excluded from the nucleolus. Importantly, we confirmed that the nucleolar
323 exclusion of TERT is not a consequence of the protein-tags used to visualize TERT in
324 these experiments. Purification of telomerase from TCAB1 knock-out cells further
325 confirmed that TCAB1 is required for telomerase assembly *in vivo*. The amount of TR and
326 dyskerin associated with TERT is substantially reduced in the absence of TCAB1. Finally,
327 we used live cell single-molecule imaging to demonstrate that the diffusion pattern of
328 TERT molecules and their interactions with telomeres are significantly different in TCAB1
329 knock-out cells compared to control cells. More importantly, TERT dynamics in the
330 absence of TCAB1 are comparable to those in TR knock-out cells where telomerase
331 assembly is impossible. Altogether, these observations support our model that TCAB1
332 promotes telomerase assembly by extracting TR from the nucleolus to facilitate its
333 assembly with TERT. Our model is further supported by work from Vogan *et al.*, which
334 demonstrated that truncated TR (hTRmin) that lacks the H/ACA region and therefore

335 cannot bind dyskerin, accumulates in the nucleoplasm and is excluded from nucleoli
336 (Vogan et al., 2016). Importantly, in cells that express hTRmin, TCAB1 is not required for
337 telomere maintenance (Vogan et al., 2016), consistent with TCAB1 promoting telomerase
338 assembly by extracting TR from the nucleolus.
339
340 **TCAB1 is not required for telomerase catalysis**
341 Previous work by others has reported conflicting results regarding the role of TCAB1 in
342 telomerase catalysis, ranging from full enzymatic activity in initial reports to substantial
343 activity defects in the most recent study (Chen et al., 2018; Venteicher et al., 2009; Vogan
344 et al., 2016). Importantly, both our work and the only other study that analyzed the role of
345 TCAB1 in telomerase activity using the "gold-standard" direct telomerase extension assay
346 concluded that telomerase activity is reduced to approximately 20-30% in the absence of
347 TCAB1. In both cases, telomerase was purified from TCAB1 knock-out cells using an
348 antibody raised against TERT prior to measuring telomerase activity. While both studies
349 concur on the degree to which telomerase activity is reduced in the absence of TCAB1,
350 the proposed underlying molecular mechanisms differ. Chen *et al*. propose that TCAB1
351 is required for proper folding of the CR4/CR5 region of the telomerase RNA, which directly
352 associates with TERT, without affecting telomerase assembly (Chen et al., 2018). Recent
353 structural analysis of the telomerase RNP from human cells revealed that TCAB1 is
354 located far away from the CR4/CR5 region of TR (Figure 6 – figure supplement 3)(Ghanim
355 et al., 2021). TCAB1 resides within the H/ACA lobe of while CR4/CR5 is located within
356 the catalytic lobe of the telomerase RNP. The two lobes are connected by the P1 and
357 P4.2 helices which can adopt multiple conformations. Importantly, TCAB1 was not located

358 near the CR4/CR5 region of TR in any of the observed telomerase RNP conformations
359 (Ghanim et al., 2021). Although it is possible that telomerase can adopt additional
360 conformations, based on the currently available structural information it is difficult to
361 rationalize a molecular mechanism by which TCAB1 could specifically promote CR4/CR5
362 folding. In addition, due to the miss-folding of TR telomerase was proposed to adopt a
363 low activity state in the absence of TCAB1. Experimentally such a low activity state would
364 manifest itself as a reduction in the specific activity of telomerase (telomerase activity per
365 assembled telomerase RNP). Our experiments strongly suggest that, while telomerase
366 assembly is reduced in the absence of TCAB1, the limited amount of telomerase that can
367 assemble is fully active (i.e. does not have reduced specific activity). Both, our enzymatic
368 analysis and the positioning of TCAB1 within the telomerase RNP do not support a role
369 of TCAB1 in TR folding and telomerase catalysis but are fully consistent with TCAB1
370 promoting telomerase assembly.
371
372 **TCAB1 is not necessary for telomerase recruitment to telomeres**
373 TCAB1 is necessary for the localization of scaRNAs to Cajal bodies and previous work
374 suggested that it is also required for telomerase recruitment to telomeres (Stern et al.,
375 2012; Venteicher et al., 2009). Our observations demonstrate that when TERT and TR
376 are overexpressed in TCAB1 knockout cells a fraction of TERT can assemble with TR an
377 localize to telomeres. Telomerase recruitment to telomeres requires a direct interaction
378 between TERT and TPP1 (Nandakumar et al., 2012; Schmidt et al., 2014; Zhong et al.,
379 2012), therefore TR that localizes to telomeres must be assembled with TERT. These
380 results are fully consistent with our model that the spatial separation of TR and TERT in

381 the absence of TCAB1 prevents telomerase assembly. When TR is overexpressed the
382 capacity of the nucleolus to sequester TR may be saturated and excess TR can assemble
383 with TERT and localize to telomeres. Importantly, our observations also suggests that
384 TCAB1 is not required for telomerase localization to telomeres.
385

386 **Molecular mechanism of telomerase RNP assembly**

387 The results presented in this study demonstrate that, in the absence of TCAB1,
388 telomerase assembly is reduced but not completely abolished. It is likely that TR bound
389 by the H/ACA complex is in an equilibrium between localizing to nucleoplasm and the
390 nucleolus. In the presence of TCAB1, this equilibrium is shifted towards the nucleoplasm
391 allowing TR to associate with TERT (Fig. 6E). In contrast, in the absence of TCAB1, the
392 majority of TR is trapped in the nucleolus effectively reducing the amount of TR that is
393 available for assembly with TERT. In addition, the nucleolus disassembles during mitosis
394 and does not reform until early G1-phase of the cell cycle (Hernandez-Verdun, 2014). In
395 cells lacking TCAB1, nucleolar disassembly should lead to the release of TR, which could
396 transiently allow telomerase assembly during cell division or prior to reformation of the
397 nucleolus in G1-phase. Both, a reduction of TR available for assembly and transient
398 assembly during cell division are plausible models to explain the limited amount of
399 telomerase that can form in the absence of TCAB1.

400 The sub-cellular location and order in which telomerase RNP components
401 associate with TR in human cells is largely unknown (Fig. 6E). Our results demonstrate
402 that telomerase does not assemble in the nucleolus. In addition, it is unlikely that
403 telomerase assembly requires intact Cajal bodies. Multiple studies have shown that

404 knock-out of coilin, which eliminates Cajal bodies, does not impact telomerase activity or
405 telomere maintenance (Chen et al., 2018; Vogan et al., 2016). Our single-molecule live
406 cell imaging of TERT has demonstrated that TERT is almost exclusively localized to the
407 nucleus, it is therefore likely that human telomerase assembles in the nucleoplasm. But
408 it cannot be ruled out that in human cells TR is transiently exported to the cytoplasm to
409 assemble with nascent TERT protein, as is the case in *S. cerevisiae* (Gallardo et al.,
410 2008).

411 The H/ACA complex has been shown to associate with scaRNAs at the site of their
412 transcription (Darzacq et al., 2006). While co-transcriptional association of the H/ACA
413 complex with TR has not been demonstrated, binding of the H/ACA complex proteins to
414 TR is likely the first step in telomerase RNP assembly, because of their critical role in TR
415 stability and 3'-end formation (Stuart et al., 2015; Tummala et al., 2015). Once TR is
416 bound to dyskerin, TR will be targeted to the nucleolus, unless it associates with TCAB1
417 (Fig. 6E). Like TERT, TCAB1 is excluded from nucleoli (Fig. 1, Fig. S2D), and dyskerin
418 an TR are localized to the dense fibrillar component (DFC, Fig. 6E) of the nucleolus (Yao
419 et al., 2019), which is separated from the nucleoplasm by the granular component (GC,
420 Fig. 6E) (Lafontaine et al., 2021). Thus, it is unlikely that TCAB1 can bind to TR localized
421 to the DFC of the nucleolus. We therefore believe that TCAB1 association with TR
422 prevents the entry of TR into the nucleolus rather than extracting TR which is already
423 localized to the DFC of the nucleolus. The association of TR with either TERT or TCAB1
424 should prevent its sequestration in the nucleolus, but the order in which TERT and TCAB1
425 bind to TR cannot be inferred from our experiments, or observation by others. Since

426 TCAB1 is substantially more abundant than TERT it is likely that TCAB1 encounters TR
427 before TERT does.
428
429 **Regulation of RNP assembly by nucleolar phase-separation**
430 In addition to the mechanistic insight into the role of TCAB1 in telomerase function, our
431 results also demonstrate that nucleolar phase separation can effectively regulate
432 telomerase RNP assembly in the nucleus of human cells. How RNA molecules are
433 specifically recruited into, excluded from, or expelled from non-membrane bound
434 organelles is a key unanswered question. One model suggests that gradual replacement
435 of non-specific, multivalent interactions of pre-ribosomal RNAs with nucleolar proteins
436 such as NPM1 and fibrillarin, with specific, high-affinity interactions with ribosomal
437 proteins leads to the ejection of mature ribosomal subunits from the nucleolus (Riback et
438 al., 2020). In this model a key driving force for the retention of RNA in the nucleolus is
439 regions of RNA not yet bound by ribosomal proteins, that are available to interact with
440 nucleolar proteins (Riback et al., 2020). By analogy, this model would explain why TR
441 bound by the H/ACA complex but not TERT would be sequestered in the nucleolus. In
442 addition to the interactions formed by the H/ACA complex with nucleolar proteins and
443 RNA, the regions of TR that are bound by TERT in the context of telomerase (i.e. the
444 pseudoknot, template, and CR4/CR5) would be available to form non-specific, multivalent
445 interactions with nucleolar proteins to strengthen the association of TR with the nucleolus
446 and prevent its release.
447 TR is a unique among the scaRNAs because it contains the additional domains
448 that associate with TERT. Most other box H/ACA scaRNAs are substantially shorter (<150

449 nucleotides) than TR (451 nucleotides), and do not contain large regions that are not
450 bound by proteins and could form non-specific interactions with nucleolar proteins. It is
451 therefore possible, that in cells lacking TCAB1, TR is strongly retained in the nucleolus
452 while other scaRNAs are less tightly bound, because they lack additional interaction sites
453 with nucleolar proteins. This provides a potential explanation for the phenotypes observed
454 in patients with TCAB1 mutations that suffer from dyskeratosis congenita. The patients
455 have a clear deficiency in telomerase function but no defects in splicing have been
456 reported (Zhong et al., 2011), which would be the consequence of complete loss of
457 scaRNA function and their critical role in spliceosome maturation.

458 How TCAB1 binding leads to the exclusion of TR and other scaRNA from the
459 nucleolus remains a key unanswered question. TCAB1 interacts with a very short
460 sequence motif in TR, which is far removed from the TR regions that associate with TERT
461 (Fig. S8) (Ghanim et al., 2021). It is therefore unlikely that TCAB1 binding leads to
462 expulsion of TR from the nucleolus by reducing the number of non-specific, multivalent
463 interactions TR can form with nucleolar proteins. As outlined above, we believe that
464 TCAB1 prevents localization of scaRNAs to the nucleolus, rather than extracting
465 scaRNAs that are already localized to the DFC. One potential explanation is that TCAB1
466 counteracts scaRNA recruitment to the nucleolus by inhibiting the nucleolar localization
467 signals within dyskerin (Heiss et al., 1999). Dissecting the molecular mechanism by which
468 TCAB1 leads to exclusion of TR from the nucleolus in future studies will undoubtably shed
469 light on the fundamental principles RNP recruitment to non-membrane bound organelles
470 and its physiological role in cell biology.
471

472 **Acknowledgements**

473 We would like to thank members of the Schmidt lab and J. Nandakumar for discussions
474 and critical reading of the manuscript and Luke Lavis (HHMI Janelia Research Campus)
475 for providing HaloTag dyes. This work was supported by a grant from the NIH (R00
476 GM120386) to J.C.S. J.C.S. is a Damon Runyon Dale F. Frey Scientist supported (in part)
477 by the Damon Runyon Cancer Research Foundation (DFS-24-17). S.B.C. acknowledges
478 sustained support from the Ernest & Piroska Major Foundation.

479

480 **Author contributions**

481 B.S.A.-M. carried out IF-FISH experiments, telomerase purifications, analyzed
482 telomerase assembly, generated mCherry- and 3xFLAG-HaloTag-dyskerin plasmids,
483 determined their sub-cellular localization, and edited the manuscript. G.I.P. maintained
484 cell lines, established TCAB1 and TR knockout cell lines and carried out IF-FISH
485 experiments. K.A.-B. assisted in establishing the TR knockout cell line and carried out
486 characterization of the TR knockout cells. S.B.C. purified and characterized the anti-TERT
487 sheep antibody. L.H. and K.Y. characterized TCAB1 knock-out clones using Southern
488 blots. J.C.S. carried out all other experiments, designed the research, analyzed data, and
489 wrote the manuscript.

490

491 **Competing interests**

492 The authors declare no competing interests.

493 **Materials and Methods**

494 **Cell Lines and Tissue Culture**

495 All cell lines were based on HeLa-EM2-11ht (Weidenfeld et al., 2009) and were cultured
496 in Dulbecco's Modified Eagle Medium including L-glutamine (Gibco) supplemented with
497 10% fetal bovine serum, 100 units/ml penicillin and 100 µg/ml streptomycin at 37°C with
498 5% CO_2. Live cell imaging was carried out using CO_2 independent media supplemented
499 with 2 mM GlutaMAX (Life Technologies), 10% fetal bovine serum, 100 units/ml penicillin
500 and 100 µg/ml streptomycin at 37°C with 5% CO_2. For single-molecule imaging of
501 HaloTag-TERT cell were cultured in homemade imaging dishes made by gluing 22x22
502 mm Nexterion coverslips (170 ± 5 µm, Schott) onto the bottom of plastic 3.5 x 1.0 cm cell
503 culture dishes with a hole in the middle using an epoxy adhesive. Prior to chamber
504 assembly the coverslips were washed with 1 M KOH and 100% for 30 min each in a
505 sonicating water bath. To enrich for cells in S-phase for live cell imaging experiments,
506 cultures we treated with complete media including 2 mM thymidine for a minimum of 16
507 hours. Cells were released 2 hours prior to imaging by replacing the thymidine containing
508 media with fresh media without thymidine. Puromycin selection was carried out at a
509 concentration of 1 µg/ml.

510

511 **Plasmid Construction and Genome Editing**

512 All plasmids were generated by Gibson assembly (NEB) using standard protocols or by
513 inverse PCR. All plasmids will be made available on Addgene. All Cas9 and sgRNA
514 expression plasmids were based on pX330 (Cong et al., 2013). The homologous
515 recombination donor for the TR knockout was generated by assembling the genomic

516 sequences immediately upstream and downstream (~500 bp each) of the TR sequence
517 flanking a puromycin resistance cassette into HpaI linearized pFastBac. The 3xFLAG-
518 HaloTag-NLS plasmids was generated by adding a 3xFLAG-tag to a previously described
519 HaloTag-NLS plasmid (a kind gift from X. Darzacq and A. Hansen) (Hansen et al., 2018).
520 The 3xFLAG-HaloTag-dyskerin plasmid was generated by replacing TERT in our
521 previously described 3xFLAG-HaloTag-TERT expression plasmid with the dyskerin
522 coding sequence (Schmidt et al., 2016). The mCherry-dyskerin plasmid was generated
523 by replacing TERT in our previously described mCherry-TERT expression plasmid with
524 the dyskerin coding sequence (Schmidt et al., 2014). All transfections were carried out
525 using Lipfectamine 2000 (Invitrogen) using the manufacturer's instructions. TCAB1 was
526 knocked-out using a single sgRNA or two separate sgRNA and Cas9 encoding plasmids
527 that were transfected alongside a GFP-expression plasmid. 24 hours after transfection
528 single-cell clones were sorted using the GFP signal. TCAB1 knock-out clones were
529 screened by PCR and confirmed by western blot, Southern Blotting of the *TCAB1* locus
530 and immunofluorescence imaging. TR was knocked out by transfecting two sgRNA
531 plasmids and a homologous recombination donor plasmid. 48 hours after transfection
532 puromycin selection was initiated and 1 week after the initiation of selection single-cell
533 clones were generated by dilution into 96-well plates. TR knock-out was confirmed using
534 PCR and Sanger sequencing, fluorescence *in situ* hybridization, and RT-qPCR.
535

536 **Immunofluorescence and Fluorescence *In Situ* Hybridization Imaging**

537 Fixed cell immunofluorescence imaging and fluorescence *in situ* hybridization was carried
538 out as previously described (Schmidt et al., 2014). Briefly, cells grown on coverslips were

539 fixed in PBS supplemented with 4% formaldehyde. When using the HaloTag for
540 fluorescence detection cells were incubated with 100 nM of JF646 HaloTag-ligand for 30
541 min prior to fixation. Unincorporated ligand was removed by 3 washes with complete
542 media followed by placing the cells back in the incubator for 10 min to let additional dye
543 leak out of the cells. mEOS3.2-TRF2 was detected using the intrinsic fluorescence of
544 green form of mEOS3.2. After removing the fixation solution using 2 PBS washes,
545 coverslips were transferred into aluminum foil covered humidity chambers with a parafilm
546 layer and rinsed with 1 ml of PBS with 0.2% Triton X-100. Cells were than incubated in
547 blocking buffer (PBS, 0.2% Triton X-100, 3% BSA) for 30 minutes, followed by incubation
548 with primary antibodies diluted in blocking buffer for 1 hour. All primary antibodies (see
549 key resource table) were used at a concentration of 1 µg/ml. After three washes with PBS
550 + 0.2% Triton X-100, coverslips were incubated with secondary antibodies diluted in PBS
551 + 0.2% Triton X-100 for 1 hour. All secondary antibodies (see key resource table) were
552 used at a concentration of 4 µg/ml. Cells were washed three times PBS + 0.2% Triton X-
553 100 prior to a second fixation with PBS + 4% formaldehyde. In cases where nuclear
554 staining was used the first of the three washing steps also included 0.1 µg/ml HOECHST.
555 After the second fixation steps coverslips were dehydrates in three steps with ethanol
556 (70%, 95%, 100%), re-hydrated in 2xSSC + 50% formamide, blocked for 1 hour in
557 hybridization buffer (100 mg/ml dextran sulfate, 0.125 mg/ml *E. coli* tRNA, 1 mg/ml
558 nuclease free BSA, 0.5 mg/ml salmon sperm DNA, 1 mM vanadyl ribonucleoside
559 complexes, 50% formamide, 2xSSC) at 37°C, before incubating the coverslips in
560 hybridization buffer supplemented with three TR probes (30 ng per coverslip) over night
561 at 37°C. Probe sequences were previously described (Tomlinson et al., 2006). After

562 hybridization coverslips were washes twice for 30 minutes in 2xSSC + 50% formamide
563 and then mounted on slides using ProLong Antifade Diamond mounting media (Life
564 Technologies). Microscopy was carried out using a DeltaVision Elite microscope using a
565 60x PlanApo objective (1.42 NA) and a pco.edge sCMOS camera. We acquired 20 Z-
566 sections spaced by 0.2 μm, followed by image deconvolution and maximum intensity
567 projection of the sections using the DeltaVision Softworx software.
568
569 **Single-Molecule Live Cell Imaging**
570 Live cell single-molecule imaging was carried out on a Olympus IX83 inverted microscope
571 equipped with a 4-line cellTIRF illuminator (405 nm, 488 nm, 561 nm, 640 nm lasers), a
572 Olympus UAPO 100x TIRF objective (1.49 NA), a CAIRN TwinCam beamsplitter, 2 Andor
573 iXon 897 Ultra EMCCD cameras, and a blacked-out environmental control enclosure. The
574 microscope was operated using the Olympus cellSense software. 3xFLAG-HaloTag-
575 TERT was labeled for 2 min in complete media supplemented with 100 nM JF646-
576 HaloTag ligand (Grimm et al., 2015). After removing the HaloTag-ligand with three
577 washes in complete media, cells were placed back in the incubator for 10 min to allow
578 unincorporated dye to leak out of the cells. Cells were then transferred into CO_2
579 independent media and put on the microscope which was heated to 37°C. Single-
580 molecule imaging was carried out at 50 or 100 frames per second using highly inclined
581 laminated optical sheet illumination (Tokunaga et al., 2008). Movies were typically 20
582 seconds in length (2000 frames) and were followed by a transmitted light acquisition to
583 visualize overall cell morphology.
584

585 **RT-qPCR**

586 RNA samples for RT-qPCR analysis were generated by using RNA mini prep kits
587 (Zymogen) using ~2 million cells as starting material. Reverse transcription was carried
588 out using random hexamer primers and SuperScript III reverse transcriptase (Invitrogen)
589 according to the manufacturer's instructions. qPCR was carried out using the Maxima
590 SYBR Green qPCR master mix (Thermo Scientific) using primers for GAPDH and TR
591 according to the manufacturer's instructions. All qPCR reactions were carried out in
592 triplicates and three independent biological replicates were analyzed.

593

594 **Southern Blotting**

595 Southern blotting was carried out using standard protocols (Southern, 2006). Briefly,
596 genomic DNA generated by phenol-chloroform extraction after cell lysis using TE
597 supplemented with 0.5% SDS and 0.1 mg/ml Proteinase K, was digested with BamHI
598 (generating a 1394 bp fragment spanning exons 1-3 of the *TCAB1* locus) and separated
599 on a 0.8% agarose gel. The DNA was then transferred on a Hybond-N+ nylon membrane
600 using capillary transfer. The *TCAB1* locus was detected using radioactive probes (alpha-
601 ^{32}P-dCTP) generated by randomly primed DNA synthesis using an 800 bp PCR product
602 overlapping with the 1394 bp restriction fragment as a template and Klenow polymerase
603 (NEB).

604

605 **Western Blotting**

606 Mini-PROTEAN TGX stain-free gels (Bio-Rad) were used for SDS-PAGE. Total protein
607 was detected using a ChemiDoc MP (Bio-Rad) after a 45 second UV activation. Western

608 transfer was carried out using the Trans-Blot Turbo transfer system (Bio-Rad) according
609 to the manufacturer's instructions using the mixed molecular weight transfer setting.
610 Immuno-blotting was carried out using standard protocols. The TCAB1 antibody
611 (Proteintech) was used at a 1:2000 dilution, the TERT antibody (Abcam) was used at a
612 1:4000 dilution, and the dyskerin antibody (Santa Cruz Biotech) was used at a 1:200
613 dilution. Secondary antibodies were used at a 1:10000 dilution.
614
615 **Northen Blotting**
616 RNA was extracted from cell lysates and purified telomerase samples supplemented with
617 10 ng of a loading and recovery control (*in vitro* transcribed TR 34-328) using the RNeasy
618 Mini kit (Qiagen) and eluted in 30 ul of RNase free water. 15 ul of eluted RNA was mixed
619 with 15 ul of 2x formamide loading buffer (0.1XTBE, 25 mM EDTA, 0.1% bromophenol
620 blue, 0.1% xylene cyanol, 93% formamide) and heated to 60 °C for 5 min. Samples were
621 separated on a 6% TBE, 7M Urea, polyacrylamide gel (Life Technologies), and
622 transferred to a Hybond N+ membrane (Cytiva) using a wet-blotting apparatus in 1x TBE
623 for 2 hours at 0.5 A of constant current in the cold room. After transfer, membranes were
624 UV-crosslinked, and pre-hybridized in Church buffer for 2 hours at 50 °C. Three DNA
625 oligos complementary to TR were radioactively labeled using T4 PNK (NEB) and ~$10x10^6$
626 cpm of each probe were added to the membrane. Hybridization was carried out at 50 °C
627 overnight. Membranes were washed three times with 2xSSC, 0.1% SDS prior to exposure
628 to a storage phosphorescence screen (Cytiva) which was then imaged on an Amersham
629 Typhoon IP phosphoimager (Cytiva).
630

631 **Telomerase Expression and Purification**

632 Cell lines were transfected in 15 cm tissue culture plates at ~90% confluency (~25-30x10^6
633 cells) using 7.5 µg of TERT plasmid, 30 µg of TR plasmid and 75 µl of Lipofectamine 2000
634 in 1875 ul of Opti-MEM (Cristofari and Lingner, 2006). Transfected cells were split to three
635 15 cm dishes 24 hours after transfection. 48 hours after transfection cells were counted,
636 harvested, and snap frozen in liquid nitrogen. Cells were lysed in 1 ml of CHAPS lysis
637 buffer supplemented with 5 µl of RiboLock RNase inhibitor (10 mM TRIS pH 7.5, 1 mM
638 $MgCl_2$, 1 mM EGTA pH 8.0, 0.5% CHAPS, 10% glycerol) per 100x10^6 cells and rotated
639 at 4 °C for 30 min. Lysates were cleared in a table-top centrifuge at 21,000xg for 15 min
640 at 4 °C. Identical cell equivalents were used for all samples. 45 µg of anti-TERT antibody
641 was added per ml of cleared lysate and samples were rotated for 1 hour at 4 °C. Lysates
642 were then added to 100 µl of protein G agarose and rotated for 1 hour at 4 °C. The resin
643 was spun down at 1000xg and washed four times with 1 ml of Buffer W (20 mM HEPES
644 pH 7.9, 300 mM KCl, 2 mM $MgCl_2$, 1 mM EDTA, 1 mM DTT, 1 mM PMSF, 0.1% Triton X-
645 100, 10% glycerol). TERT was eluted in 100 µl of Buffer W supplemented with 5 µl of 1
646 mM TERT peptide by rotating for 30 min at room temperature.

647

648 **Telomerase Activity Assays**

649 Telomerase assays were carried out in 20 µl of reaction buffer (50 mM TRIS pH 8.0, 150
650 mM KCl, 1 mM MgCl2, 2 mM DTT, 100 nM TTAGGGTTAGGGTTAGG oligo, 10 µM dATP,
651 10 µM dGTP, 10 µM dTTP, 0.165 µM dGTP [α-32P] 3000 Ci/mmol) including 2 µl of
652 purified telomerase for 1 hour at 30 °C. Telomerase was incubated with the substrate
653 oligo for 15 min at room temperature, prior to initiating the reaction by addition of dNTPs.

654 Reactions were stopped by adding 100 µl of 3.6 M of ammonium acetate supplemented
655 with 20 µg of glycogen and 32P 5'-end labeled loading control oligos
656 (TTAGGGTTAGGGTTAGGG, TTAGGGTTAGGGTTAG). Reaction products were
657 precipitated using 500 µl of ice-cold ethanol and stored at -20 °C over-night. Reaction
658 products were spun down in a table-top centrifuge at max speed for 30 min at 4 °C,
659 washed with 500 µl of 70% ethanol, and spun down again speed for 30 min at 4 °C. The
660 70% ethanol was decanted, and the reaction products were dried in an Eppendorf
661 vacuum concentrator at 45 °C. Reaction products were resuspended in 20 µl of loading
662 buffer (0.05XTBE, 25 mM EDTA, 0.05% bromophenol blue, 0.05% xylene cyanol, 46.5%
663 formamide) and incubated at 95 °C for 5 min. 10 µl of each sample was separated on a
664 12% polyacrylamide, 7 M urea sequencing gel pre-run for 45 min at 90W. Gels were dried
665 and exposed to a storage phosphorescence screen (Cytiva) and imaged on an
666 Amersham Typhoon IP phosphoimager (Cytiva).
667
668 **Single-Particle Tracking**
669 Single-particle tracking was carried out in MATLAB 2019a using a batch parallel-
670 processing version of SLIMfast modified to allow the input of TIFF files (kindly provided
671 by Xavier Darzacq and Anders Hansen) (Hansen et al., 2018), an implementation of the
672 Multiple-Target-Tracing algorithm (Sergé et al., 2008), with the following settings:
673 Exposure Time = 10 ms, NA = 1.49, Pixel Size = 0.16 µm, Emission Wavelength = 664
674 nm, D_{max} = 5 $\mu m^2/s$, Number of gaps allowed = 2, Localization Error = 10^{-5}, Deflation
675 Loops = 0. Diffusion coefficients and the fraction of molecules in each distinct particle
676 population were determined using the MATLAB version of the Spot-On tool (kindly

677 provided by Xavier Darzacq and Anders Hansen) (Hansen et al., 2018) with the following
678 settings: TimeGap = 10 ms or 20 ms, dZ = 0.700 µm, GapsAllowed = 2, TimePoints = 8,
679 JumpsToConsider = 4, BinWidth = 0.01 µm, PDF-fitting, D_Free1_3State = [1 25],
680 D_Free2_3State = [0.1 1], D_Bound_3State = [0.0001 0.1]. For all experiments we carried
681 out 3 independent biological replicates with at least 15 cells for each cell line. The
682 complete data set can be found in supplemental figure S6D. The statistical significance
683 of differences in particle fractions and diffusion coefficients were assessed using a two-
684 tailed T-Test.
685
686 **Quantification of Fixed Cell Imaging**
687 For the quantification of cellular TR distribution in control and TCAB1 knockout cells we
688 assigned cells into one of three categories: Cells with TR only at telomeres, Cells with TR
689 only in nucleoli, Cells with TR at telomeres and in nucleoli. We carried out 3 independent
690 biological replicates and counted a minimum of 100 cells for control and TCAB1 knockout
691 cells.
692
693 **Quantification of RT-qPCR data**
694 RT-qPCR experiments were carried out in triplicate and the TR Ct value was normalized
695 to the GAPDG Ct value. The mean ΔCt (Ct of TR – Ct of GAPDH) value from three
696 independent experiments and the corresponding standard deviation is shown in figure
697 S3B.
698
699 **Quantification of Western Blots, Northern Blots, and Telomerase Activity Assays**

700 Gel images from Western Blots, Northern Blots, and Telomerase Activity Assays were
701 analyzed using ImageQuant TL 8.2. To quantify TR levels in Northern blots the TR band
702 intensity was normalized to the loading and recovery control signal added to the RNA
703 sample prior to RNA purification. To quantify telomerase activity the whole lane intensity
704 starting at repeat 1 was determined and divided by the sum of the loading control signals.
705 Telomerase processivity was calculated by dividing product intensity > 7 repeats by the
706 total signal in the respective lane. The statistical significance of the observed differences
707 was calculated using a two-tailed T-test using a minimum of three biological replicates.
708 Each biological replicate (independent telomerase expression and purification) was
709 analyzed in technical triplicate.
710
711

712 **References**

713 Angrisani A, Vicidomini R, Turano M, Furia M. 2014. Human dyskerin: beyond
714 telomeres. *Biol Chem* **395**:593–610. doi:10.1515/hsz-2013-0287

715 Armanios M, Blackburn EH. 2012. The telomere syndromes. *Nat Rev Genet* **13**:693
716 704. doi:10.1038/nrg3246

717 Chen L, Roake CM, Freund A, Batista PJ, Tian S, Yin YA, Gajera CR, Lin S, Lee B,
718 Pech MF, Venteicher AS, Das R, Chang HY, Artandi SE. 2018. An Activity Switch in
719 Human Telomerase Based on RNA Conformation and Shaped by TCAB1. *Cell* **174**.
720 doi:10.1016/j.cell.2018.04.039

721 Cohen SB, Graham ME, Lovrecz GO, Bache N, Robinson PJ, Reddel RR. 2007. Protein
722 Composition of Catalytically Active Human Telomerase from Immortal Cells. *Science*
723 **315**:1850–1853. doi:10.1126/science.1138596

724 Cong L, Ran FA, Cox D, Lin S, Barretto R, Habib N, Hsu PD, Wu X, Jiang W, Marraffini
725 LA, Zhang F. 2013. Multiplex Genome Engineering Using CRISPR/Cas Systems.
726 *Science* **339**:819–823. doi:10.1126/science.1231143

727 Cristofari G, Lingner J. 2006. Telomere length homeostasis requires that telomerase
728 levels are limiting. *Embo J* **25**:565 574. doi:10.1038/sj.emboj.7600952

729 Darzacq X, Kittur N, Roy S, Shav-Tal Y, Singer RH, Meier UT. 2006. Stepwise RNP
730 assembly at the site of H/ACA RNA transcription in human cells. *J Cell Biology*
731 **173**:207–218. doi:10.1083/jcb.200601105

732 Freund A, Zhong FL, Venteicher AS, Meng Z, Veenstra TD, Frydman J, Artandi SE.
733 2014. Proteostatic Control of Telomerase Function through TRiC-Mediated Folding of
734 TCAB1. *Cell* **159**:1389 1403. doi:10.1016/j.cell.2014.10.059

735 Gallardo F, Olivier C, Dandjinou AT, Wellinger RJ, Chartrand P. 2008. TLC1 RNA
736 nucleo-cytoplasmic trafficking links telomerase biogenesis to its recruitment to
737 telomeres. *Embo J* **27**:748 757. doi:10.1038/emboj.2008.21

738 Ghanim GE, Fountain AJ, Roon A-MM van, Rangan R, Das R, Collins K, Nguyen THD.
739 2021. Structure of human telomerase holoenzyme with bound telomeric DNA. *Nature*
740 1–5. doi:10.1038/s41586-021-03415-4

741 Grimm JB, English BP, Chen J, Slaughter JP, Zhang Z, Revyakin A, Patel R, Macklin
742 JJ, Normanno D, Singer RH, Lionnet T, Lavis LD. 2015. A general method to improve
743 fluorophores for live-cell and single-molecule microscopy. *Nat Methods* **12**:244 50–3
744 p following 250. doi:10.1038/nmeth.3256

745 Hansen AS, Woringer M, Grimm JB, Lavis LD, Tjian R, Darzacq X. 2018. Robust
746 model-based analysis of single-particle tracking experiments with Spot-On. *Elife* **7**.
747 doi:10.7554/elife.33125

748 Heiss NS, Girod A, Salowsky R, Wiemann S, Pepperkok R, Poustka A. 1999. Dyskerin
749 Localizes to the Nucleolus and Its Mislocalization Is Unlikely to Play a Role in the
750 Pathogenesis of Dyskeratosis Congenita. *Hum Mol Genet* **8**:2515–2524.
751 doi:10.1093/hmg/8.13.2515

752 Hernandez-Verdun D. 2014. Assembly and disassembly of the nucleolus during the cell
753 cycle. *Nucleus* **2**:189–194. doi:10.4161/nucl.2.3.16246

754 Hyman AA, Weber CA, Jülicher F. 2014. Liquid-Liquid Phase Separation in Biology.
755 *Annu Rev Cell Dev Bi* **30**:39–58. doi:10.1146/annurev-cellbio-100913-013325

756 Jády BE, Bertrand E, Kiss T. 2004. Human telomerase RNA and box H/ACA scaRNAs
757 share a common Cajal body–specific localization signal. *J Cell Biology* **164**:647–652.
758 doi:10.1083/jcb.200310138

759 Lafontaine DLJ, Riback JA, Bascetin R, Brangwynne CP. 2021. The nucleolus as a
760 multiphase liquid condensate. *Nat Rev Mol Cell Bio* **22**:165–182.
761 doi:10.1038/s41580-020-0272-6

762 Mitrea DM, Kriwacki RW. 2016. Phase separation in biology; functional organization of a
763 higher order. *Cell Commun Signal Ccs* **14**:1. doi:10.1186/s12964-015-0125-7

764 Nagpal N, Wang J, Zeng J, Lo E, Moon DH, Luk K, Braun RO, Burroughs LM, Keel SB,
765 Reilly C, Lindsley RC, Wolfe SA, Tai AK, Cahan P, Bauer DE, Fong YW, Agarwal S.
766 2020. Small-Molecule PAPD5 Inhibitors Restore Telomerase Activity in Patient Stem
767 Cells. *Cell Stem Cell* **26**:896-909.e8. doi:10.1016/j.stem.2020.03.016

768 Nandakumar J, Bell CF, Weidenfeld I, Zaug AJ, Leinwand LA, Cech TR. 2012. The TEL
769 patch of telomere protein TPP1 mediates telomerase recruitment and processivity.
770 *Nature* **492**:285 289. doi:10.1038/nature11648

771 Nandakumar J, Cech TR. 2013. Finding the end: recruitment of telomerase to
772 telomeres. *Nat Rev Mol Cell Bio* **14**. doi:10.1038/nrm3505

773 Riback JA, Zhu L, Ferrolino MC, Tolbert M, Mitrea DM, Sanders DW, Wei M-T, Kriwacki
774 RW, Brangwynne CP. 2020. Composition-dependent thermodynamics of intracellular
775 phase separation. *Nature* **581**:209–214. doi:10.1038/s41586-020-2256-2

776 Schmidt JC, Cech TR. 2015. Human telomerase: biogenesis, trafficking, recruitment,
777 and activation. *Gene Dev* **29**:1095 1105. doi:10.1101/gad.263863.115

778 Schmidt JC, Dalby AB, Cech TR. 2014. Identification of human TERT elements
779 necessary for telomerase recruitment to telomeres. *Elife* **3**:e03563.
780 doi:10.7554/elife.03563

781 Schmidt JC, Zaug AJ, Cech TR. 2016. Live Cell Imaging Reveals the Dynamics of
782 Telomerase Recruitment to Telomeres. *Cell* **166**:1188 1197.e9.
783 doi:10.1016/j.cell.2016.07.033

784 Schmidt JC, Zaug AJ, Kufer R, Cech TR. 2018. Dynamics of human telomerase
785 recruitment depend on template-telomere base pairing. *Mol Biol Cell* **29**:869 880.
786 doi:10.1091/mbc.e17-11-0637

787 Sergé A, Bertaux N, Rigneault H, Marguet D. 2008. Dynamic multiple-target tracing to
788 probe spatiotemporal cartography of cell membranes. *Nat Methods* **5**:687 694.
789 doi:10.1038/nmeth.1233

790 Shukla S, Jeong H-C, Sturgeon CM, Parker R, Batista LFZ. 2020. Chemical inhibition of
791 PAPD5/7 rescues telomerase function and hematopoiesis in dyskeratosis congenita.
792 *Blood Adv* **4**:2717–2722. doi:10.1182/bloodadvances.2020001848

793 Shukla S, Schmidt JC, Goldfarb KC, Cech TR, Parker R. 2016. Inhibition of telomerase
794 RNA decay rescues telomerase deficiency caused by dyskerin or PARN defects. *Nat*
795 *Struct Mol Biol* **23**:286 292. doi:10.1038/nsmb.3184

796 Southern E. 2006. Southern blotting. *Nat Protoc* **1**:518–525. doi:10.1038/nprot.2006.73

797 Stern JL, Zyner KG, Pickett HA, Cohen SB, Bryan TM. 2012. Telomerase Recruitment
798 Requires both TCAB1 and Cajal Bodies Independently. *Mol Cell Biol* **32**:2384–2395.
799 doi:10.1128/mcb.00379-12

800 Stewart SA, Weinberg RA. 2006. Telomeres: Cancer to Human Aging. *Annu Rev Cell*
801 *Dev Bi* **22**:531–557. doi:10.1146/annurev.cellbio.22.010305.104518

802 Stuart BD, Choi J, Zaidi S, Xing C, Holohan B, Chen R, Choi M, Dharwadkar P, Torres
803 F, Girod CE, Weissler J, Fitzgerald J, Kershaw C, Klesney-Tait J, Mageto Y, Shay
804 JW, Ji W, Bilguvar K, Mane S, Lifton RP, Garcia CK. 2015. Exome sequencing links
805 mutations in PARN and RTEL1 with familial pulmonary fibrosis and telomere
806 shortening. *Nat Genet* **47**:512 517. doi:10.1038/ng.3278

807 Tokunaga M, Imamoto N, Sakata-Sogawa K. 2008. Highly inclined thin illumination
808 enables clear single-molecule imaging in cells. *Nat Methods* **5**:159 161.
809 doi:10.1038/nmeth1171

810 Tomlinson RL, Ziegler TD, Supakorndej T, Terns RM, Terns MP. 2006. Cell cycle-
811 regulated trafficking of human telomerase to telomeres. *Mol Biol Cell* **17**:955 965.
812 doi:10.1091/mbc.e05-09-0903

813 Tseng C-K, Wang H-F, Burns AM, Schroeder MR, Gaspari M, Baumann P. 2015.
814 Human Telomerase RNA Processing and Quality Control. *Cell Reports* **13**:2232–
815 2243. doi:10.1016/j.celrep.2015.10.075

816 Tummala H, Walne A, Collopy L, Cardoso S, Fuente J de la, Lawson S, Powell J,
817 Cooper N, Foster A, Mohammed S, Plagnol V, Vulliamy T, Dokal I. 2015. Poly(A)-
818 specific ribonuclease deficiency impacts telomere biology and causes dyskeratosis
819 congenita. *J Clin Invest* **125**:2151–2160. doi:10.1172/jci78963

820 Venteicher AS, Abreu EB, Meng Z, McCann KE, Terns RM, Veenstra TD, Terns MP,
821 Artandi SE. 2009. A human telomerase holoenzyme protein required for Cajal body
822 localization and telomere synthesis. *Science* **323**:644 648.
823 doi:10.1126/science.1165357

824 Vogan JM, Zhang X, Youmans DT, Regalado SG, Johnson JZ, Hockemeyer D, Collins
825 K. 2016. Minimized human telomerase maintains telomeres and resolves
826 endogenous roles of H/ACA proteins, TCAB1, and Cajal bodies. *Elife* **5**:693.
827 doi:10.7554/elife.18221

828 Weidenfeld I, Gossen M, Löw R, Kentner D, Berger S, Görlich D, Bartsch D, Bujard H,
829 Schönig K. 2009. Inducible expression of coding and inhibitory RNAs from
830 retargetable genomic loci. *Nucleic Acids Res* **37**:e50. doi:10.1093/nar/gkp108

831 Wu RA, Upton HE, Vogan JM, Collins K. 2017. Telomerase Mechanism of Telomere
832 Synthesis. *Annu Rev Biochem* **86**:439 460. doi:10.1146/annurev-biochem-061516-
833 045019

834 Xi L, Cech TR. 2014. Inventory of telomerase components in human cells reveals
835 multiple subpopulations of hTR and hTERT. *Nucleic Acids Res* **42**:8565–8577.
836 doi:10.1093/nar/gku560

837 Yao R-W, Xu G, Wang Ying, Shan L, Luan P-F, Wang Yang, Wu M, Yang L-Z, Xing Y-
838 H, Yang L, Chen L-L. 2019. Nascent Pre-rRNA Sorting via Phase Separation Drives
839 the Assembly of Dense Fibrillar Components in the Human Nucleolus. *Mol Cell*
840 **76**:767-783.e11. doi:10.1016/j.molcel.2019.08.014

841 Zhong F, Savage SA, Shkreli M, Giri N, Jessop L, Myers T, Chen R, Alter BP, Artandi
842 SE. 2011. Disruption of telomerase trafficking by TCAB1 mutation causes
843 dyskeratosis congenita. *Gene Dev* **25**:11–16. doi:10.1101/gad.2006411

844 Zhong FL, Batista LFZ, Freund A, Pech MF, Venteicher AS, Artandi SE. 2012. TPP1
845 OB-Fold Domain Controls Telomere Maintenance by Recruiting Telomerase to
846 Chromosome Ends. *Cell* **150**:481 494. doi:10.1016/j.cell.2012.07.012

847

Supplementary Information

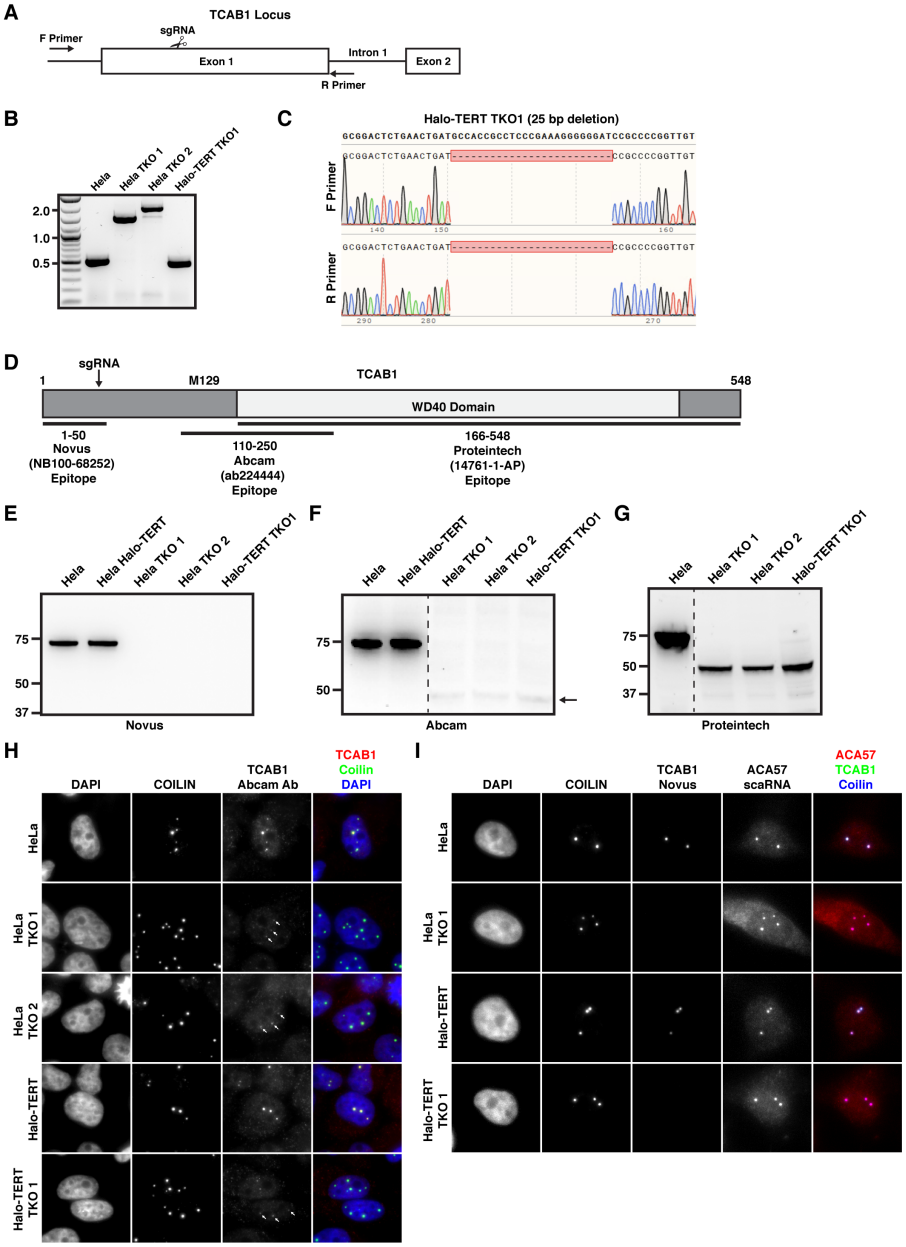

Figure 1 – Figure Supplement 1. (A) Strategy to knock-out TCAB1 with a single Cas9 and a single sgRNA targeting exon 1 of the *TCAB1* gene. **(B)** PCR of TCAB1 knock-out clones using the primers indicated in **(A)** demonstrating the absence of a WT *TCAB1* allele. **(C)** Sanger sequencing of the PCR product derived from Halo-TERT TKO1 **(B)** demonstrating deletion causing a frame shift. **(D)** Model of TCAB1 protein indicating the antigens used to raise the indicated TCAB1 antibodies. **(E-G)** Western blots of parental cells and TCAB1 knock-out clones using **(E)** the Novus Biological, **(F)** Abcam, and **(G)** Proteintech TCAB1 antibodies, demonstrating the presence of a truncated TCAB1 protein in the putative TCAB1 knock-out cells. **(H)** IF using antibodies against coilin and TCAB1 (Abcam) demonstrating that truncated TCAB1 can be detected in Cajal bodies (white arrows) in putative TCAB1 knock-out clones. **(I)** IF using coilin and TCAB1 (Novus Biologicals) antibodies coupled to FISH with probes against the scaRNA ACA57, demonstrating that the Novus Biologicals antibody fails to detect the truncated TCAB1 and scaRNA localization is unchanged in putative TCAB1 knock-out cells.

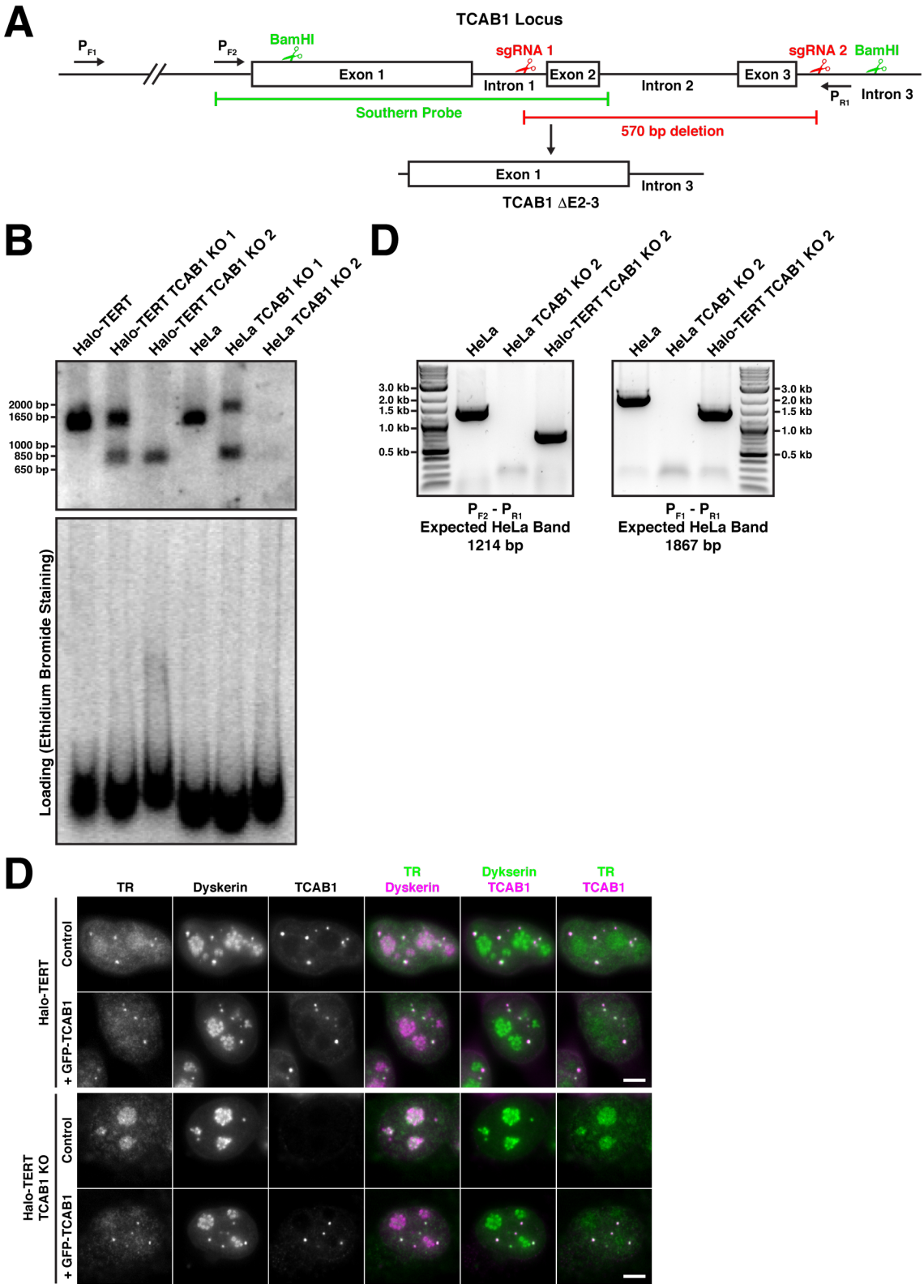

Figure 1 – Figure Supplement 2. (A) Strategy to knock-out TCAB1 using Cas9 and two sgRNAs targeting introns 1 and 3. **(B)** Southern blot of genomic DNA digested with BamHI from parental cells and TCAB1 knock-out clones using a probes generated from a PCR product of the TCAB1 gene indicated in **(A)** demonstrating the expected truncation of the *TCAB1* gene in Halo-TERT TCAB1 KO 2. HeLa TCAB1

867 KO 2 carries larger deletions completely removing exons 1 and 2 from the *TCAB1* gene. **(C)** PCR using
868 primers indicated in **(A)** of genomic DNA from parental cells and TCAB1 knock-out clones confirming the
869 deletion of critical regions of the *TCAB1* gene show in **(B)**. **(D)** Immuno-fluorescence with anti-dyskerin
870 and anti-TCAB1 antibodies coupled to fluorescence in-situ hybridization with probes against TR,
871 demonstrating that expression of GFP-TCAB1 in TCAB1 knockout cells rescues TR localization to Cajal
872 bodies (scale bar = 5 μm).
873

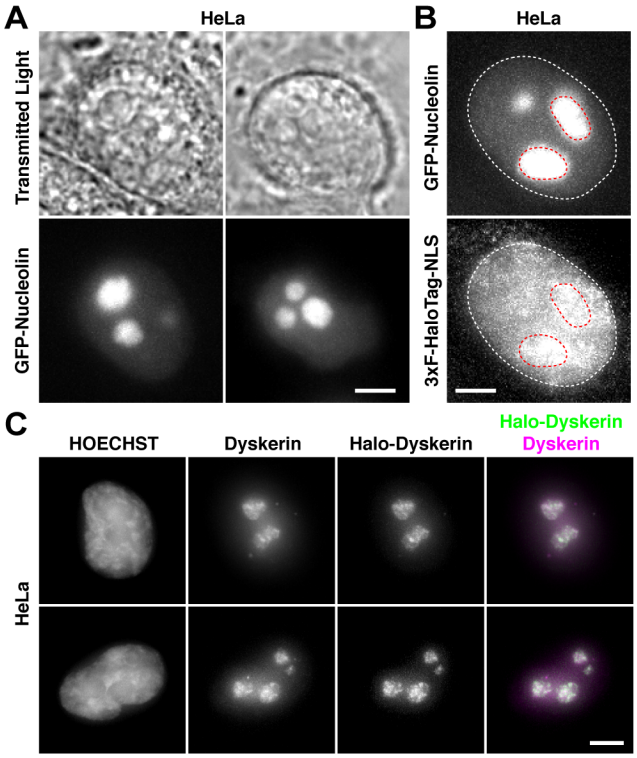

874

875 **Figure 2 – Figure Supplement 1. (A)** Images of HeLa cells transiently expressing GFP-nucleolin to mark
876 nucleoli. The GFP-nucleolin signal overlaps with circular shapes visible under transmitted light illumination
877 (scale bar = 2 μm). **(B)** Images of HeLa cells transiently expressing GFP-nucleolin and 3xFLAG-HaloTag-
878 NLS labeled with JF646. The 3xFLAG-HaloTag-NLS signal (maximum intensity projection of 1000 frames
879 of a single-molecule imaging movie) clearly overlaps with the GFP-nucleolin signal (red dashed outline),
880 demonstrating that 3xFLAG-HaloTag-NLS can enter the nucleolus (scale bar = 2 μm). **(C)** Images of HeLa
881 cells transiently expressing 3xFLAG-HaloTag-dyskerin labeled with JF646 and probed with an antibody
882 against dyskerin, demonstrating that 3xFLAG-HaloTag-dyskerin localizes to the nucleolus (scale bar = 5
883 μm).

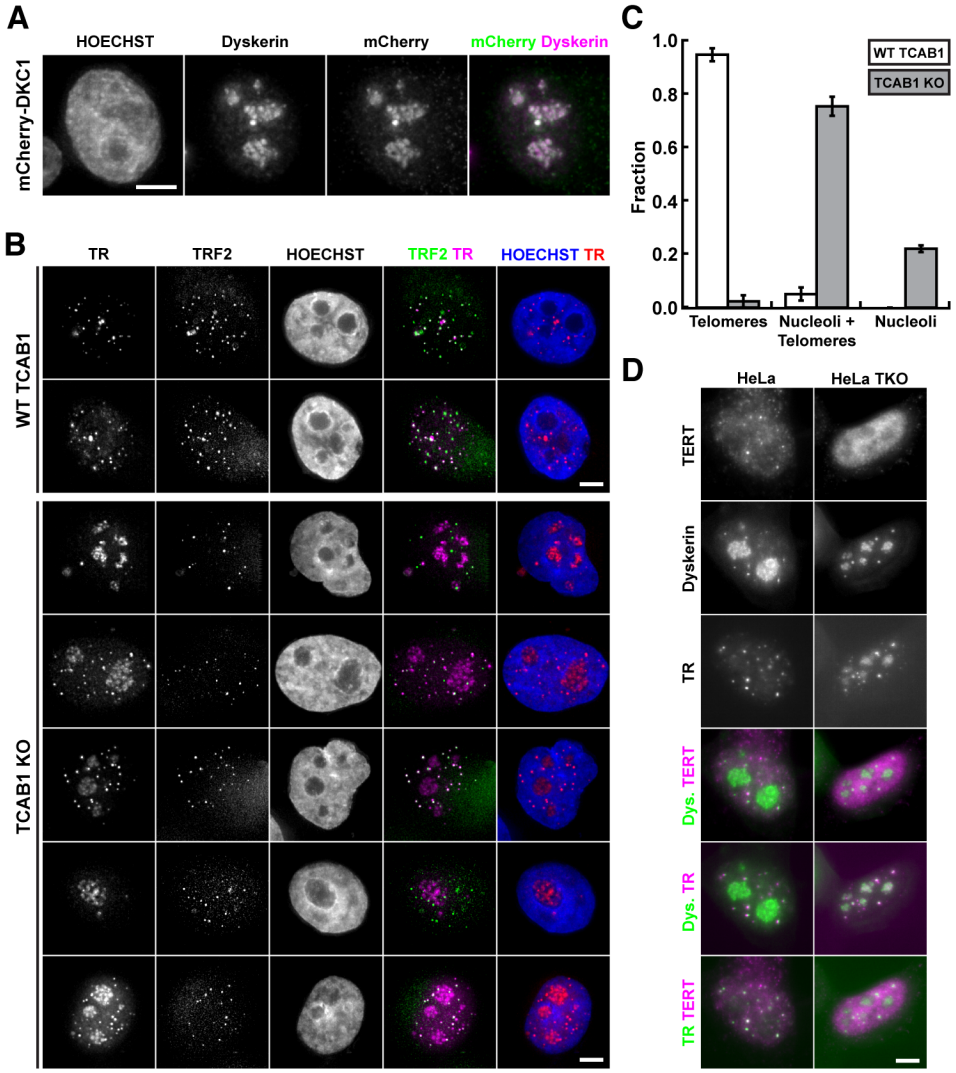

Figure 3 – Figure Supplement 1. (A) Images of HeLa cells transiently expressing mCherry-dyskerin probed with antibodies agains mCherry and dyskerin, demonstrating that mCherry dyskerin localizes to the nucleolus (scale bar = 5 μm). **(B)** Images of control and TCAB1 knock-out HeLa cells (3xFLAG-Halo-TERT, mEOS3.2-TRF2) overexpressing untagged TERT and TR. TR was detected using FISH and TRF2 was visualized using the fluorescence signal from mEOS3.2-TRF2. In control cells TR co-localizes with telomeres, while it is enriched in nucleoli and localized to telomeres in TCAB1 KO cells (scale bar = 5 μm). **(C)** Quantification of the fraction of cells showing TR localization exclusively to telomeres, to telomeres and nucleoli, or only to nucleoli (2 independent experiments, >100 cells per experiments, mean ± standard deviation). **(D)** Images of HeLa cells and TCAB1 knockout cells transiently expressing untagged TERT and TR, probed with TERT (Abcam) and dyskerin antibodies and FISH for TR demonstrating that untagged TERT is excluded from nucleoli marked by dyskerin in parental and TCAB1 knock-out cells.

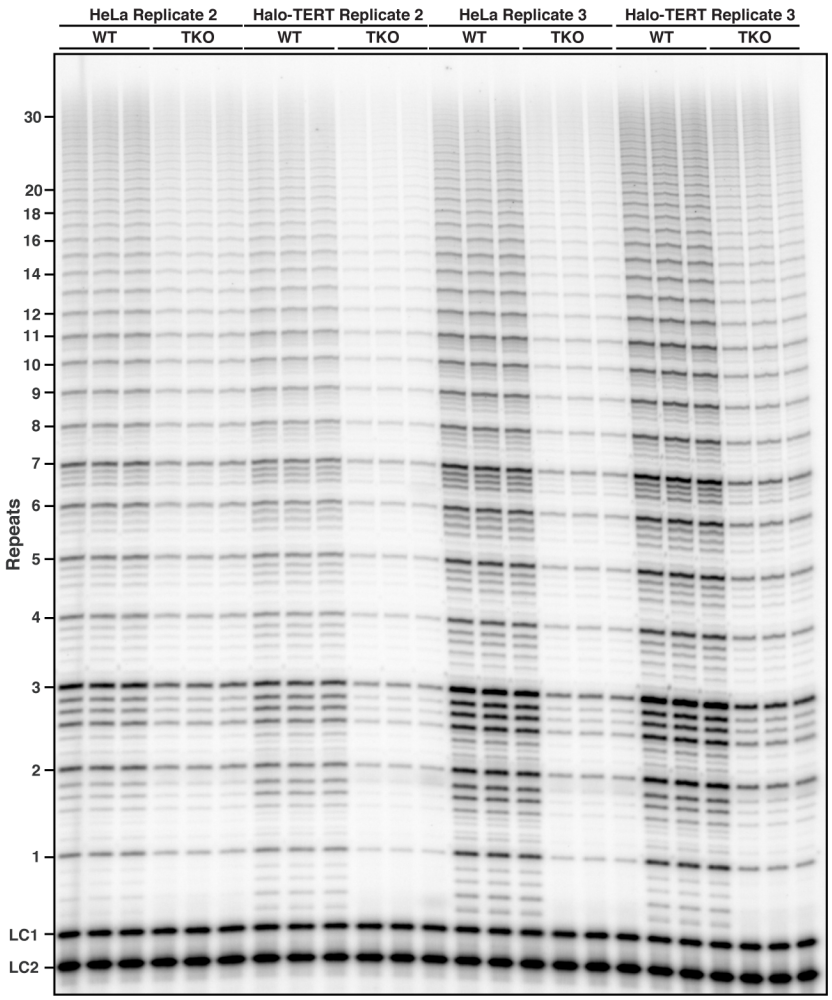

Figure 5 – Figure Supplement 1. Direct telomerase extension assay of telomerase immuno-purified from parental (WT) and TCAB1 knock-out (TKO) HeLa and Halo-TERT cell lines. LC1 and LC2, radiolabeled DNA oligonucleotide loading controls.

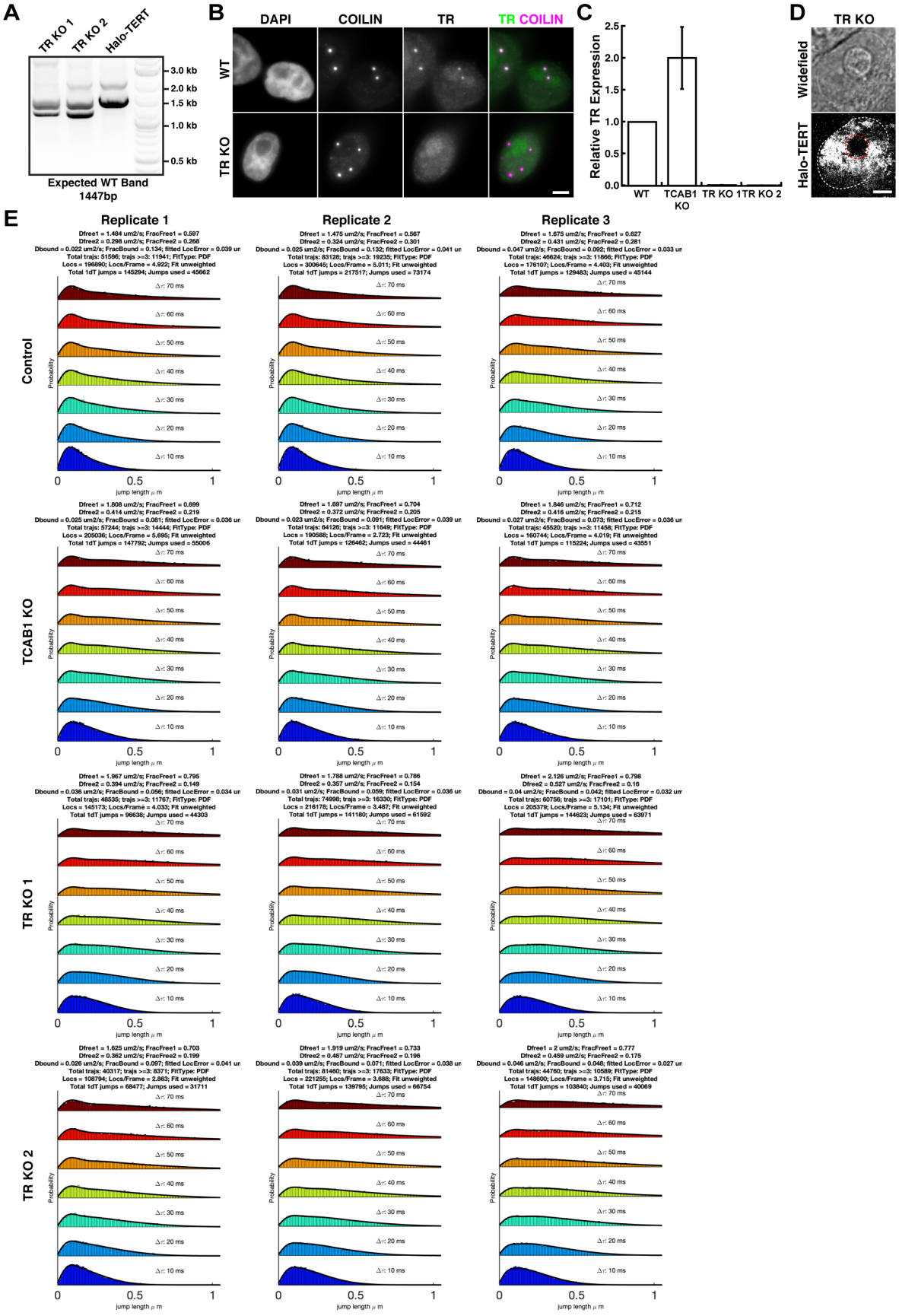
A
TR KO 1
TR KO 2
Halo-TERT
3.0 kb
2.0 kb
1.5 kb
1.0 kb
0.5 kb
Expected WT Band
1447bp
B
DAPI
COILIN
TR
TR COILIN
WT
TR KO
C
Relative TR Expression
2.5
2.0
1.5
1.0
0.5
0.0
WT
TCAB1 KO
TR KO 1
TR KO 2
D
TR KO
Widefield
Halo-TERT
E
Replicate 1
Replicate 2
Replicate 3
Control
TCAB1 KO
TR KO 1
TR KO 2
Probability
jump length μ m
Δτ: 70 ms
Δτ: 60 ms
Δτ: 50 ms
Δτ: 40 ms
Δτ: 30 ms
Δτ: 20 ms
Δτ: 10 ms

903

904 **Figure 6 – Figure Supplement 1. (A)** PCR analysis of the TR locus in parental and TR knock-out clones.
905 Both TR knock-out clones show PCR products with reduced length that were confirmed to be knock-outs
906 by Sanger sequencing. **(B)** Images of control and TR knock-out cells probed with an antibody against
907 coilin and FISH probes specific for TR, demonstrating the lack of TR signal in TR knock-out cells (scale
908 bar = 5 μm). **(C)** Determination of TR levels in control, TCAB1 knock-out, and TR knock-out cells, using
909 RT-qPCR with primers specific to TR normalized to GAPDH (3 independent biological replicates, 3
910 technical replicates for each biological replicate, mean ± standard deviation). **(D)** Maximum intensity
911 projection of 2000 frames of a 3xFLAG-HaloTag (JF646) TERT movie (bottom), demonstrating that the
912 TERT signal does not overlap with the nucleolus detected as circular shape in the transmitted light image
913 (top, red dashed line). **(E)** Fitting of single-particle tracking data of TERT from control, TCAB1 knock-out,
914 and TR knock-out cells expressing 3xFLAG-HaloTag-TERT using the Spot-On tool.
915
916

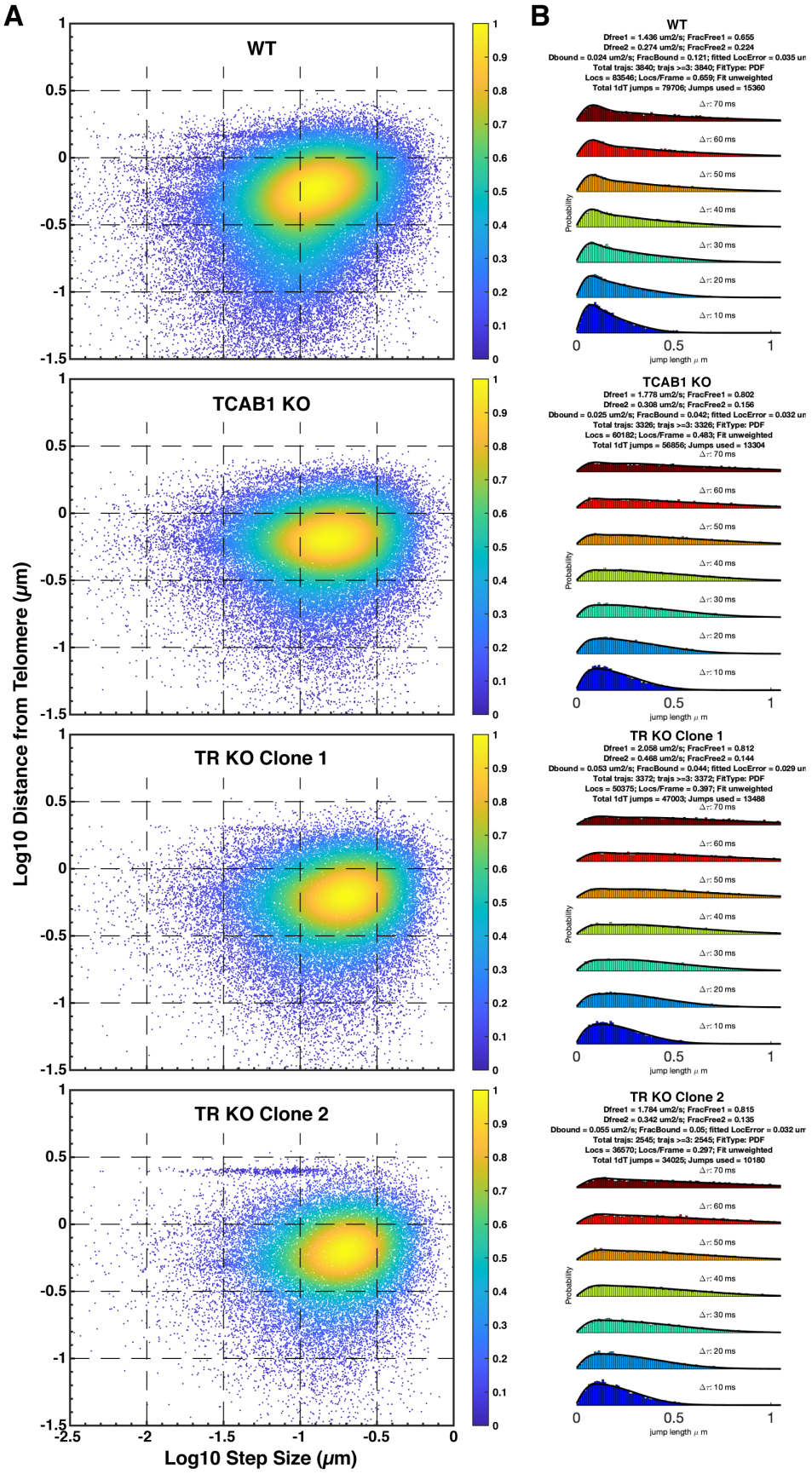
A
B
WT
TCAB1 KO
TR KO Clone 1
TR KO Clone 2
Log10 Distance from Telomere (μm)
Log10 Step Size (μm)
Dfree1 = 1.436 um2/s; FracFree1 = 0.655
Dfree2 = 0.274 um2/s; FracFree2 = 0.224
Dbound = 0.024 um2/s; FracBound = 0.121; fitted LocError = 0.035 um
Total trajs: 3840; trajs >=3: 3840; FitType: PDF
Locs = 83546; Locs/Frame = 0.659; Fit unweighted
Total 1dT jumps = 79706; Jumps used = 15360
Dfree1 = 1.778 um2/s; FracFree1 = 0.802
Dfree2 = 0.308 um2/s; FracFree2 = 0.156
Dbound = 0.025 um2/s; FracBound = 0.042; fitted LocError = 0.032 um
Total trajs: 3326; trajs >=3: 3326; FitType: PDF
Locs = 60182; Locs/Frame = 0.483; Fit unweighted
Total 1dT jumps = 56856; Jumps used = 13304
Dfree1 = 2.058 um2/s; FracFree1 = 0.812
Dfree2 = 0.468 um2/s; FracFree2 = 0.144
Dbound = 0.053 um2/s; FracBound = 0.044; fitted LocError = 0.029 um
Total trajs: 3372; trajs >=3: 3372; FitType: PDF
Locs = 50375; Locs/Frame = 0.397; Fit unweighted
Total 1dT jumps = 47003; Jumps used = 13488
Dfree1 = 1.784 um2/s; FracFree1 = 0.815
Dfree2 = 0.342 um2/s; FracFree2 = 0.135
Dbound = 0.055 um2/s; FracBound = 0.05; fitted LocError = 0.032 um
Total trajs: 2545; trajs >=3: 2545; FitType: PDF
Locs = 36570; Locs/Frame = 0.297; Fit unweighted
Total 1dT jumps = 34025; Jumps used = 10180
Δτ: 70 ms
Δτ: 60 ms
Δτ: 50 ms
Δτ: 40 ms
Δτ: 30 ms
Δτ: 20 ms
Δτ: 10 ms
Probability
jump length μ m

917

Figure 6 – Figure Supplement 2. (A) Analysis if the step size of telomeric TERT particles relative to the distance of the particle to the closest telomere (pooled results from 3 independent biological replicates with 19-30 cells analyzed per replicate). TERT molecules bound to the telomere are expected to have small step sizes and a short distance to the closest telomere, which is apparent in the enrichment of events in the lower quadrants in the WT control. This enrichment is not observed in TCAB1 and TR knock-out cells. **(B)** Spot-On analysis of telomeric TERT particles (pooled results from 3 independent biological replicates with 19-30 cells analyzed per replicate). The fraction of bound TERT particles in TCAB1 and TR knock-out cells is 4-5%, compared to 12% in the WT control cells.

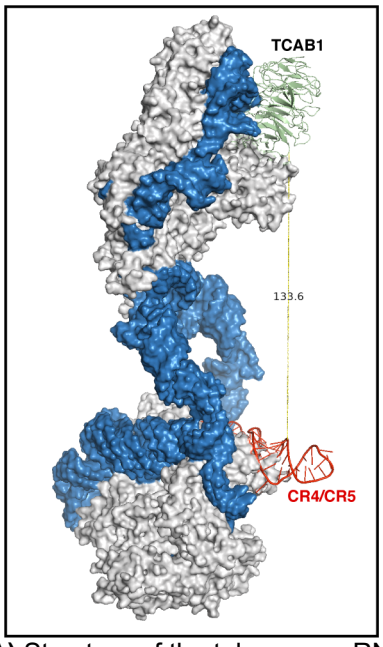

Figure 6 – Figure Supplement 3. (A) Structure of the telomerase RNP showing the distance between TCAB1 and CR4/CR5 (13.4 nm). TR in blue, CR4/CR5 in red, and TCAB1 in green (Ghanim et al., 2021).

932 **Movie Legends**
933
934 **Movie 1.** Single-particle tracking of 3xFLAG-HaloTag-TERT labeled with JF646 in a
935 control cell acquired at 100 frames per second. Trajectories with a minimum of 5
936 localizations are displayed. 150x150 pixels with a pixel size of 0.16 μm.
937
938 **Movie 2.** Single-particle tracking of 3xFLAG-HaloTag-TERT labeled with JF646 in a
939 TCAB1 knockout cell acquired at 100 frames per second. Trajectories with a minimum of
940 5 localizations are displayed. 150x150 pixels with a pixel size of 0.16 μm.
941
942 **Movie 3.** Movie of cell expressing GFP-nucleolin (red) and 3xFLAG-HaloTag-NLS (green)
943 labeled with JF646 acquired at 100 frames per second, showing overlap of 3xFLAG-
944 HaloTag-NLS with nucleoli. 140x140 pixels with a pixel size of 0.16 μm.
945
946 **Movie 4.** Movie of 3xFLAG-HaloTag-TERT labeled with JF646 in a control (left), TCAB1
947 knockout (middle), and TR knockout (right) cell acquired at 100 frames per second. Each
948 panel is 150x150 pixels in size with a pixel size of 0.16 μm.
949
950 **Movie 5.** Single-particle tracking of 3xFLAG-HaloTag-TERT labeled with JF646 in a TR
951 knockout cells acquired at 100 frames per second. Trajectories with a minimum of 5
952 localizations are displayed. 150x150 pixels with a pixel size of 0.16 μm.
953
954